SSI-DT46205028

Doctor Thesis

A study on design optimization and anomaly detection of wireless power transfer

Yunyi Gong

A dissertation submitted in partial fulfillment
Of the requirements for the degree of
Doctor of Information Science

Course of Systems Science and Informatics
Graduate School of Information Science and Technology
Hokkaido University

Doctor Thesis
Submitted to Graduate School of Information Science and Technology
Hokkaido University
In partial fulfillment of the requirements for the degree of
Doctor of Information Science

Yunyi Gong

Thesis Committee:	**Professor**	**Hajime IGARASHI (Chief examiner)**
	Professor	**Satoshi OGASAWARA**
	Professor	**Hiroyuki KITA**
	Associate Professor	**So NOGUCHI**

SSI-DT46205028

A study on design optimization and anomaly detection of wireless power transfer

Yunyi Gong

Abstract

In recent decades, wireless power transfer (WPT) has been attracting more and more attention of researchers for its potential as charging system of electrical vehicles and consumer electronics. Proposed one century ago, the most classical theory of WPT – inductive coupling – has been developed a lot, realizing plenty of applications in several areas. Except for the unchanged main objective of transfer efficiency, the safety of WPT system is also important, especially when WPT become practical. Among the works of safety of WPT, the reduction of leakage electromagnetic radiation, and the detection and removal of foreign object are the main purposes. In addition, the effect of coil-misalignment on these performances need to be considered and reduced, as another aspect of anomaly detection of WPT other than foreign object.

In this paper, several researches aiming at these purposes will be introduced. Lots of thoughts and methods from the areas different from electromagnetism and power electronic have been used, to promote the improvement of WPT further.

In chapter 2, works of design optimization of magnetic core in WPT coupler are introduced. In order to obtain brand new optimized shape, topology optimization is used, which can express more complicated shapes that designer is hard to imagine, than parameter optimization. For the expression of topology shape, normalized gaussian network (NGnet) method is applied, in which the topology shape can be described and controlled by discrete variables, allowing us to use evolutionary algorithm to solve the optimization problem. In this way, the topology optimizations

have been implemented in the designs of magnetic core in couplers with circular coil, double-D coil, and H-shape core. For each of them, reference models are prepared and compared with the optimized results, to see if the latter have better performances on the objectives they are considering.

In chapter 3, except for the magnetic core, the shape of transmitting coil is considered as the object of design optimization. Based on a multi-layer coils system with a simple individual input control strategy, the shapes of coils are optimized using target field method, considering transfer efficiency and leakage magnetic field simultaneously, under different coil-misalignment conditions. Obtained by evolutionary algorithm as well, the optimized results are compared with the reference model, showing stronger anti-misalignment performance.

In chapter 4, we shift attention to foreign object detection in WPT. Concerning the potential fire risk brought by invaded metal object, a metal object detection (MOD) method is proposed. Based on feature signals extracted from WPT system, MOD is realized by machine learning methods, in which the detection is treated as classification problem. To implement MOD for different WPT coupler, detection coils are introduced to get more feature signals which can help represent the status of system. Meanwhile, position prediction of receiving coil is realized at the same time, which can be helpful for WPT system to adjust the performances on efficiency and leakage field. Finally, both the MOD and position prediction have been evaluated and show good accuracy.

Keywords: wireless power transfer, topology optimization, evolutionary algorithm, metal object detection, machine learning.

List of Contents

Abstract i
List of Contents iii
List of Figures v
List of Tables vii
Chapter 1 Introduction 1
1.1 Background 1
1.2 Purposes 2
1.3 Thesis Outline 2
Chapter 2 Topology optimization of magnetic core in WPT coupler 4
2.1 Wireless power transfer 4
2.1.1 Coupler in WPT 5
2.1.2 Equivalent circuit of inductive coupling WPT 6
2.2 Topology optimization 8
2.2.1 Normalized Gaussian network method 10
2.3 Optimization algorithm 11
2.3.1 Genetic Algorithm 12
2.4 Single-objective optimization 18
2.4.1 H-shape core 18
2.4.2 DD-shaped coil 21
2.5 Multi-objective optimization 27
2.5.1 Circular coil 28
2.5.2 DD coil 31
2.6 Conclusion 34
Chapter 3 Optimizations of transmitting coil in WPT coupler 35
3.1 Multi-layers coil and control-strategy 36
3.2 Target field method 38
3.3 NGnet method 40
3.4 Optimization setting 41
3.5 Optimization result 43
3.6 Conclusion 45
Chapter 4 Metal object detection and coil misalignment prediction in WPT system 46
4.1 Object detection to classification problem 47

4.2 Machine learning methods 50
4.2.1 Support vector machine (SVM) 50
4.2.2 Naive Bayes classifier (NBC) 51
4.2.3 Gradient boosting decision tree (GBDT) 51
4.2.4 Random forest classifier (RFC) 52
4.2.4 Neural network (NN) 52
4.3 Sensorless metal object detection for WPT without magnetic core 54
4.3.1 WPT system and simulation 54
4.3.2 machine learning classifiers 56
4.3.3 Classification results (simulation) 56
4.3.4 Classification results (experiment) 57
4.3.5 Conclusion 61
4.4 Metal object detection for WPT with magnetic core 61
4.4.1 WPT system model 62
4.4.2 Simulations 63
4.4.3 data preparation and machine learning 65
4.4.4 Training and validation 67
4.4.5 Conclusion 71
4.5 MOD and misalignment prediction together 71
4.5.1 WPT system model 72
4.5.2 Data preparation 73
4.5.2 Neural network 75
4.5.3 Training and validation 76
4.5.4 Conclusion 81
Chapter 5 Conclusion 82
5.1 Topology optimization for WPT coupler 82
5.2 Optimization for transmitting coils 82
5.3 Metal object detection and position prediction 83
References 85
Acknowledgement 90
Research Achievements 92
Journal 92
International conference 92
Domestic conference 93

List of Figures

Fig. 2.1 wireless power transfer....5
Fig. 2.2 representative coupler shapes....6
Fig. 2.3 equivalent circuit of inductive coupling WPT....7
Fig. 2.4 parameter optimization....8
Fig. 2.5 Topology optimization....9
Fig. 2.6 Normalized Gaussian network (NGnet) ©2020 IOS Press....10
Fig. 2.7 On/off method process....11
Fig. 2.8 process of typical genetic algorithm....13
Fig. 2.9 process of micro-GA....15
Fig. 2.10 Pareto front....17
Fig. 2.11 Coupler with H-shaped core....18
Fig. 2.12 Reference model (H-shaped core coupler)....20
Fig. 2.13 Optimized results (H-shaped core coupler)....20
Fig. 2.14 Coupler with DD-coil....22
Fig. 2.15 simulation model (DD-coil coupler)....22
Fig. 2.16 Optimized results (DD-coil coupler)....23
Fig. 2.17 Leakage reducing design of DD-coil....25
Fig. 2.18 NGnet placement....26
Fig. 2.19 optimized model....26
Fig. 2.20 Circular coil....28
Fig. 2.21 Diagram and arrangement of Gaussians (circular) ©2020 IOS Press....29
Fig. 2.22 Pareto front of optimization for circular coupler ©2020 IOS Press....30
Fig. 2.23 Reference model and optimized models (Circular) ©2020 IOS Press....31
Fig. 2.24 Diagram and arrangement of Gaussians (DD) ©2020 IOS Press....32
Fig. 2.25 Pareto front of optimization for DD coupler ©2020 IOS Press....33
Fig. 2.26 Reference model and optimized models (DD) ©2020 IOS Press....33
Fig. 3.1 WPT system....37
Fig. 3.2 Multi-layer coils control-strategy....38
Fig. 3.3 NGnet setting for coils....40
Fig. 3.4 Observation area of leakage magnetic field....42
Fig. 3.5 Calculation process....43
Fig. 3.6 Optimized coil designs....44

Fig. 3.7 Reference coil design 44
Fig. 4.1 The model of WPT coils 48
Fig. 4.2 Loci of input impedances 49
Fig. 4.3 Loci of input impedances 50
Fig. 4.4 Gradient boosting decision tree © 2022 Japan Society for Simulation Technology 51
Fig. 4.5 Multilayer perceptron 52
Fig. 4.6 WPT system model © 2021 Emerald Publishing Limited 54
Fig. 4.7 Impedance loci (simulation) © 2021 Emerald Publishing Limited 55
Fig. 4.8 Structure of NN © 2021 Emerald Publishing Limited 56
Fig. 4.9 Experiment devices © 2021 Emerald Publishing Limited 57
Fig. 4.10 Impedance loci (experiment, cylinder) © 2021 Emerald Publishing Limited 59
Fig. 4.11 Impedance loci (experiment, can) © 2021 Emerald Publishing Limited 60
Fig. 4.12 Impedance loci (experiment, key) © 2021 Emerald Publishing Limited 61
Fig. 4.13 WPT model © 2022 Japan Society for Simulation Technology 62
Fig. 4.14 Differential induced voltages at 75 kHz for different cases 64
Fig. 4.15 Differential induced voltages at 85 kHz for different cases 65
Fig. 4.16 Differential induced voltages at 100 kHz for different cases 65
Fig. 4.17 Process of proposed method 66
Fig. 4.18 Visualizations of classification by SVD 71
Fig. 4.19 WPT system model © 2022 IEEE 72
Fig. 4.20 WPT coupler © 2022 IEEE 72
Fig. 4.21 Differential coils © 2022 IEEE 73
Fig. 4.22 Visualization of $\{Vp\}$ through SVD © 2022 IEEE 75
Fig. 4.23 NN structure 76
Fig. 4.24 Dependence of performance on number of cases for the 15-turn model 77
Fig. 4.25 Dependence of misalignment distance error in the *x, y,* and clearance variation in *z* on the number of cases (15turns, without MOD) © 2022 IEEE 79

List of Tables

Table 2.1 Parameters of WPT system and coupler 19
Table 2.2 micro-GA parameters 19
Table 2.3 Comparison of optimized and reference model 21
Table 2.4 Parameters of WPT system and coupler 23
Table 2.5 Comparison results (DD-coil coupler) 24
Table 2.6 Average results of optimizations 24
Table 2.7 Comparison results 26
Table 2.8 Parameters of WPT system and NSGA-II 30
Table 3.1 Parameters of MO-CMA-ES 42
Table 3.2 Performances comparison (optimized model / reference model) 45
Table 4.1 Parameters of WPT 55
Table 4.2 value of $\gamma 2 = 1\sigma 2$ 56
Table 4.3 Accuracy of three methods for validation data (simulations) 57
Table 4.4 Accuracy of three methods for validation data (experiment, cylinder) 58
Table 4.5 Accuracy of three methods for validation data (experiment, can) 59
Table 4.6 Accuracy of three methods for validation data (experiment, key) 60
Table 4.7 Hyper parameters and setting of GBDT 67
Table 4.8 Hyper parameters and setting of RFC 67
Table 4.9 Accuracy of trained classifiers 68
Table 4.10 Hyperparameter of the NN 76
Table 4.11 MOD accuracy and error in position prediction of trained NN 78
Table 4.12 Accuracy and error in position prediction of trained NN (without MOD) 80
Table 4.13 Accuracy for MOD and position prediction under noisy environment (15 turns) 81

Chapter 1 Introduction

In this chapter, the background, purposes of the researches, and the outline of this thesis will be described.

1.1 Background

In recent years, the increasing concerns of the global warming and air pollution has stimulated the research of electric vehicles (EV). However, in the application of EV, lots of issues needs to be solved or improved, such as the energy storage and charging. For energy charging, compared to conventional solutions like wired plug-in system, wireless power transfer (WPT) is considered as a possible alternative with potential for its relative advantages like ease of operation.

The origin of WPT dates back to the turn of the 20th century, when Nikola Tesla proposed a short and midrange WPT system based on inductive coupling [1], making a profound impact on even modern WPT applications. Since then, WPT basing on different theories has been proposed, like capacitive coupling [2] and microwaves [3]. However, inductive coupling still attracts attentions and realized practicality successfully such as Qi standard [4]. The major performances of a WPT system includes system's efficiency, safety, and robustness to charging environment changing, especially the position misalignment. To improve these, the relative researches cover areas as circuit design, electromagnetic compatibility, control theory, electromagnetic computation and more. Specifically, lots of design of couplers with various structure has been proposed and developed in consideration of different performance and usage scenario, through magnetic flux route design, which will be elaborated in next chapter.

As for the optimization method for electric device and machine, parameter optimization is the usually used method. Nevertheless, parameter optimization depends strongly on the designer's

experience to decide the design parameters, which determines that it's hard for parameter optimization to find novel structure or shape in design region. Differing from that, topology optimization, expressing design shape without explicit variables, is considered to have a stronger ability on searching for complicated novel design shape [5], though it usually causes larger difficulty of actual production.

1.2 Purposes

In this study, several works are proposed to make improvement on the performances and safety of WPT system through different methods. To be specified, following issues will be discussed in this thesis.

1. 3D topology optimization of H-shape magnetic core and core for double D (DD) shaped coils.
2. Multi-objective topology optimization of magnetic core for circular and DD shaped coils.
3. Multi-objective optimization of coil shape using target field method.
4. Foreign metallic object detection in WPT system.
5. Coil misalignment distance prediction.

1.3 Thesis Outline

This thesis is organized as follows:

Chapter 1: Introduction

Describe the research background and purposes of this thesis.

Chapter 2: Topology optimization2 of magnetic core in WPT coupler

The expression method of topology and optimizers used in the optimizations are introduced. Then the optimization results for different couplers and objective functions are described and discussed.

Chapter 3: Optimizations of transmitting coil in WPT coupler

Target field method is introduced firstly, following by the descriptions of optimizer and optimization problem setting in the work. Next, the optimization results under different problem setting are compared, to see the effect towards the robustness of system to coil misalignment.

Chapter 4: Metal object detection and coil misalignment prediction in WPT system

The idea of machine learning model construction for MOD and misalignment prediction is introduced, together with the used machine learning method. The performances of proposed method are evaluated using simulation and experiments data respectively.

Chapter 5: Conclusions

Give a summary of the researches and forecast the future research direction.

Chapter 2 Topology optimization of magnetic core in WPT coupler

In this chapter, the research background and basic theory of WPT will be introduced in detail firstly, following by that of topology optimization. Then, the proposed works are going to be introduced in turn.

2.1 Wireless power transfer

As mentioned in Chapter 1, the researches of wireless power transfer have lasted for over a century. Based on different theories, several methods for WPT have been proposed. As described in Fig. 2.1, theories of WPT can be basically divided into two types, which are based on electromagnetic wave and mechanical wave [6] respectively, of which the former is more popular. And the WPT based on electromagnetic mainly insist of far-field methods, inductive coupling, and capacitive coupling. The far-field methods including microwave [7] and laser [8], usually have the characteristics such as long transfer distance, high input power, low efficiency, and high risk of safety. By comparison, the two near field methods – inductive and capacitive coupling, have relatively short transfer distance and high efficiency. While the capacitive coupling WPT [9], using the electric field between metal plates to deliver energy, still needs developments to solve issues like short transfer distance and safety risk due to strong electric field. However, inductive coupling is the type which is most popular and plenty of applications in industry. Except for Qi standard, which is mentioned in chapter 1, inductive coupling WPT is widely used in charging EV and industrial devices as well. Especially, due to the rapid development and mature application of EV, plenty of attentions are attracted on the development of inductive coupling WPT, which is considered as the most possible alternative of traditional wired charging system.

In this thesis, the WPT system for EV based on inductive coupling is mainly considered and discussed. The basic structure of coupler and circuit of inductive coupling WPT system will be introduced in this chapter.

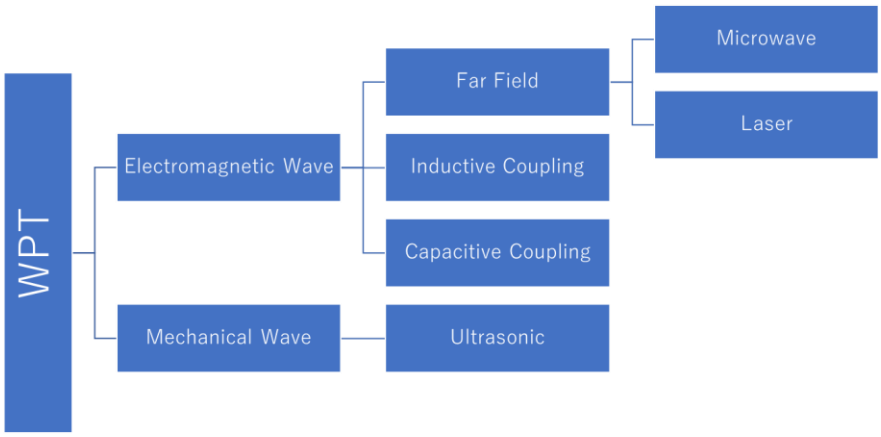

Fig. 2.1 wireless power transfer

2.1.1 Coupler in WPT

In this decade, lots of researches of WPT for EV have been proposed, while the design of coupler shape is an important issue that decides the basic features of WPT system like the electromagnetic field distribution, and the merits and weakness in performances. Three representative coupler shapes which are considered in this thesis are shown in Fig. 2.2. Generally, a WPT coupler consists of coil and magnetic core which are colored as yellow and grey in Fig. 2.2. The magnetic core, usually applying material like ferrite, is implemented near the coil to enhance the coupling between the couplers to obtain longer transfer distance and higher transfer efficiency.

Among these three designs, circular coil is first proposed design, and has advantages like simplicity. Lots of works have been proposed to optimize the design of circular, including the size of coil and the shapes of magnetic core [10]. Nevertheless, circular coil has weakness of short transfer distance and low tolerance to misalignment between couplers, which raise the

requirements for new design to overcome such weakness. Thus, Double-D coil was proposed, showing better tolerance to misalignment because of its different flux patterns derived from two D-shaped coil [11]. Coupler with H-shaped core was proposed with similar purpose – improve tolerance to misalignment by changing flux pattern [12]. Based on these two coupler shapes, several works have been proposed to optimize the designs for better performances [13]-[15].

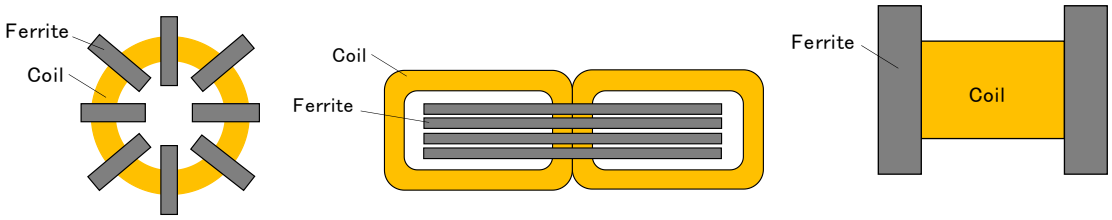

(a) Circular coil (b) Double-D coil (c) H-shaped core

Fig. 2.2 representative coupler shapes

2.1.2 Equivalent circuit of inductive coupling WPT

In Fig. 2.3, the equivalent circuit of a basic inductive coupling WPT system is shown, where I_1, R_1 and L_1 represent the input source, equivalent resistance, and self-inductance of primary coupler, while R_2, L_2 and R_L denote the equivalent resistance and self-inductance of secondary coupler, and load resistance of system respectively. And M is the mutual inductance between primary and secondary coupler. For such system, the coupling coefficient, which represent the coupling effect between two couplers, is defined as:

$$k = \frac{\sqrt{L_1 L_2}}{M} \tag{2.1}$$

In electromagnetic simulation, the self-inductances of couplers can be calculated by equation (2.2), and mutual inductance can be obtained by equation (2.3).

$$N_i \Phi_i = L_i I_i \tag{2.2}$$

$$V_2 = j\omega M I_1 \tag{2.3}$$

where N_i, Φ_i and I_i represent the number of turns in coil, magnetic flux through the coils, and current in coils respectively, while the index i denote the side number of couplers. In equation

(2.3), V_2 and ω are the induced voltage on secondary coil and angular frequency of the WPT system.

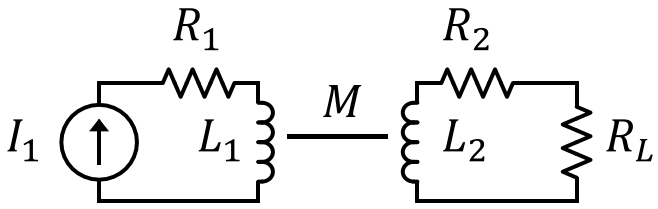

(a) Non-resonance type

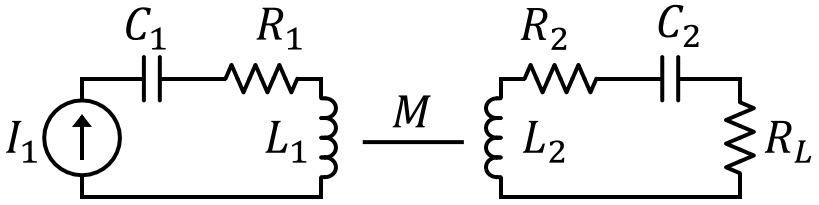

(b) Resonance type (series-series)

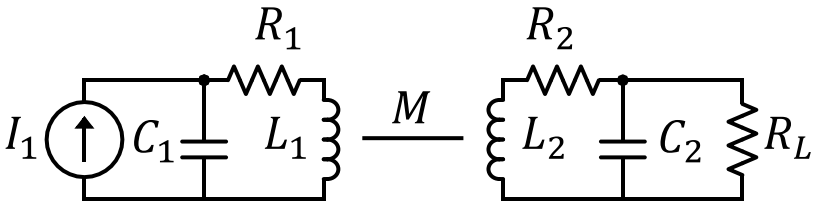

(c) Resonance type (parallel- parallel)

Fig. 2.3 equivalent circuit of inductive coupling WPT

Above the basic inductive coupling system shown as Fig. 2.3 (a), capacitor is often added in series of parallel with coils, as shown in Fig. 2.3 (b), (c). Some of Tesla's early work have described and discussed such magnetic resonance system [16]. However, the theory of magnetic resonance WPT is still based on inductive coupling, and the introduction of capacitor is for reducing or canceling the leakage inductance. By this way, the mutual inductance effect and efficiency in such loosely coupled system can be improved. The resonance frequency of the WPT system can be calculated according to equation (2.4). In general, the resonance frequency of

primary and secondary side of WPT system need to be adjusted to the same value.

$$f_{resonance} = \frac{1}{2\pi\sqrt{LC}} \tag{2.4}$$

For EV charging system, as noted in standards [[17], [18]], the resonance frequency – the operating frequency of system as well – is specified between 79 to 90 kHz, of which 85 kHz is the most common frequency.

2.2 Topology optimization

As mentioned above, optimization is a necessary and important work to complete the development of electrical device. After the basic design scheme is proposed, the details like shape, size, and system parameters need to be optimized for obtaining better performance, where parameter optimization is usually considered to solve such problems.

Generally, the parameter optimization problem can be described as followings:

$$min. \leftarrow f(\boldsymbol{v_i}) \tag{2.5}$$

where $f(\boldsymbol{v_i})$ is an implicit function with variables $\boldsymbol{v_i}$, and the objective function of the optimization problem. For example, in shape optimization problem, as illustrated in Fig. 2.4, by adjusting $\boldsymbol{v_i}$, the shape of design object which is marked as blue, can be changed accordingly. Besides that, parameter optimization for system parameters like operating frequency and capacitance is also often considered in WPT system design [19].

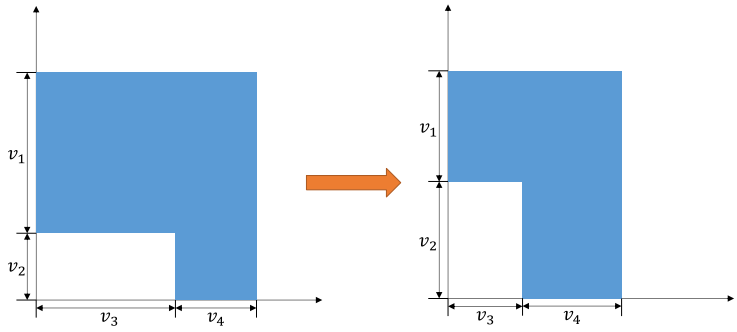

Fig. 2.4 parameter optimization

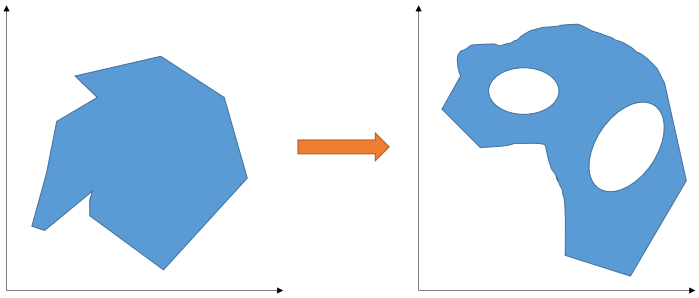

Fig. 2.5 Topology optimization

Different to parameter optimization, topology optimization is another way to consider shape optimization problem. As shown in Fig. 2.5, topology usually tend to express more novel shape that is hard for designer to imagine and describe in the form of explicit shape parameters as shown in Fig. 2.4. In order to find more shapes that have better performance, topology optimization have attracted more and more attention in optimization design for electrical device [20]. Plenty of works of optimizing different devices have been proposed, such as electrical motor [5], antenna [22], and WPT coupler [22].

Since last century, lots of methodologies have been proposed to solve topology optimization problems. Density method [23] and level-set method [24] are the representative methods which have been widely used in structural design and electromagnetic device design. In recent years, Normalized Gaussian network on/off method (NGnet on/off method) has attracted a lot of attentions for its good shape expressing ability and simplicity of calculation. It has been applied in topology optimizations of many different devices, and was proved effective for those problems [[5], [22]]. The works in this chapter are based on NGnet on/off method as well, and the introduction of it will be given in next section.

2.2.1 Normalized Gaussian network method

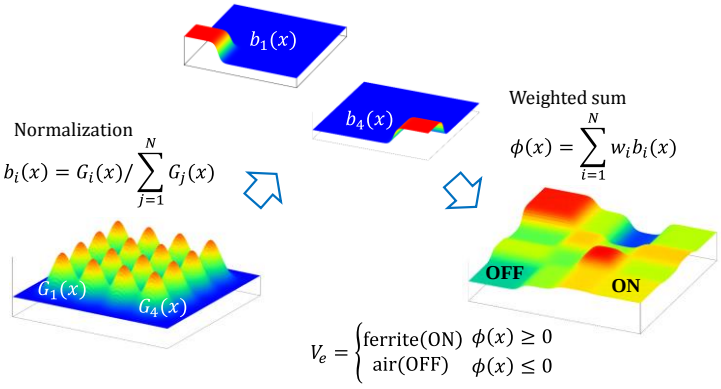

Fig. 2.6 Normalized Gaussian network (NGnet) ©2020 IOS Press

In this section, NGnet method will be introduced in detail, together with the application of it in on/off topology optimization problem.

As shown in Fig. 2.6, firstly, lots of Gaussian functions are placed over the design region, while the amount and distribution of them are decided by designer. For each Gaussian function, the calculation is described as equation (2.7). Then, the Gaussian functions are normalized as equation (2.6), before the topology shape function can be calculated by equation (2.8).

$$G_i(\boldsymbol{x}) = \frac{1}{(2\pi)^{\frac{D}{2}}\sigma^D} \exp\left(-\frac{1}{2\sigma^2}|\boldsymbol{x} - \boldsymbol{\mu_i}|^2\right) \tag{2.6}$$

$$b_i = \frac{G_i(\boldsymbol{x})}{\sum_{j=1}^{N_g} G_j(\boldsymbol{x})} \tag{2.7}$$

Where $G_i(\boldsymbol{x})$ and b_i represent the i-th gaussian function and normalized gaussian function. D, σ, $\boldsymbol{\mu_i}$ in (2.6) denote the dimensions of gaussian function, standard deviation, and the center coordinate of i-th gaussian function respectively. While N_g in (2.6) is the amount of gaussian functions placed over the design region. Then, the shape function ϕ can be obtain as following:

$$\phi(\boldsymbol{x}) = \sum_{j=1}^{N_g} w_i b_i(\boldsymbol{x}) \tag{2.8}$$

where w_i is the weight coefficient for i-th normalized gaussian function b_i. By this way, ϕ appears like what is shown in Fig. 2.6, which consists of somewhat discrete and flat hills and

valleys.

In this thesis, only two material problem is considered, for which the material of each element in mesh is defined as (2.9), where the two materials correspond to on or off state.

$$V_e = \begin{cases} \text{on} & \phi(\boldsymbol{x_e}) \geq 0 \\ \text{off} & \phi(\boldsymbol{x_e}) \leq 0 \end{cases} \tag{2.9}$$

where $\boldsymbol{x_e}$ and V_e denote the center coordinate of element and the on/off state.

So far, the material distribution of design region can be expressed by NGnet method, and adjusted by simply controlling the weight coefficients w_i. Moreover, in electromagnetic simulation by Finite Element Method (FEM), the simulation objects with the extended air region need to be meshed, consisting many elements and nodes. Here, applying NGnet on on/off method, like what is described in (2.9), the relationship between the material of each element in design region and the coefficients weights has been built. Then the topology optimization problem can be expressed in a similar form with parameter optimization, which is described in (2.5).

In Fig. 2.7, a rough process of topology optimization using on/off method is illustrated. Starting from a random initial state shown in the left, adjusting the material distribution of the elements, a different topology with optimized performance on the objective functions is finally obtained as the right.

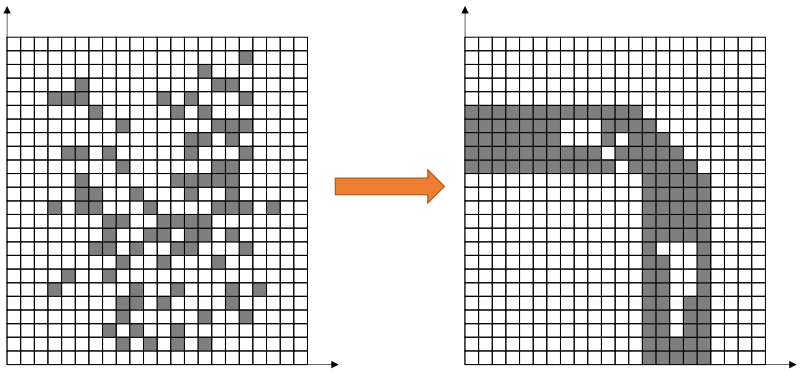

Fig. 2.7 On/off method process

2.3 Optimization algorithm

In the previous section, the background of topology optimization, and the methods for expressing

topology have been introduced. Following that, the optimization algorithms to solve such optimization problems defined like (2.5) are going to be introduced in this section.

Traditionally, gradient methods are usually adopted to settle with such minimization problems, like what is in [[23], [24]]. However, this approach requires that the relationship between objective functions and optimization variables can be expressed and calculated numerically. But in some cases, the considered problem cannot satisfy this requirement, or the calculation is complicated and time-consuming, making unpractical. Especially, in electromagnetic simulation by FEM, the simulation model can have up to millions of elements in three-dimensional problem, which makes the simulation and optimization time-consuming. Therefore, without requirement of explicit numerical expression, evolutionary algorithms such as genetic algorithm (GA), differential evolution (DA), and particle swarm optimization (PSO) were deployed to solve topology optimization problem, and showed good performances [[5], [15], [22]].

Because GA is the algorithm adopted in the works reported in this chapter to solve the optimization problems, only the introduction of GA is going to be given in this chapter. There are some other algorithms which are used in other works in this thesis, and the introduction of those algorithms will be given when those works are reported.

2.3.1 Genetic Algorithm

In this section, a typical process of GA will be introduced firstly. Then, several modified types of GA used in the published works will be introduced respectively.

The idea of GA is inspired by the process of natural selection. In GA, the optimization variables are set as the genes in chromosome of individuals. During the optimization, crossover and mutation happen on the genes from time to time to generate new individuals with new genes. Finally, with the evolution of the whole population advancing towards the direction of better genes, the individuals with better performances can be obtained.

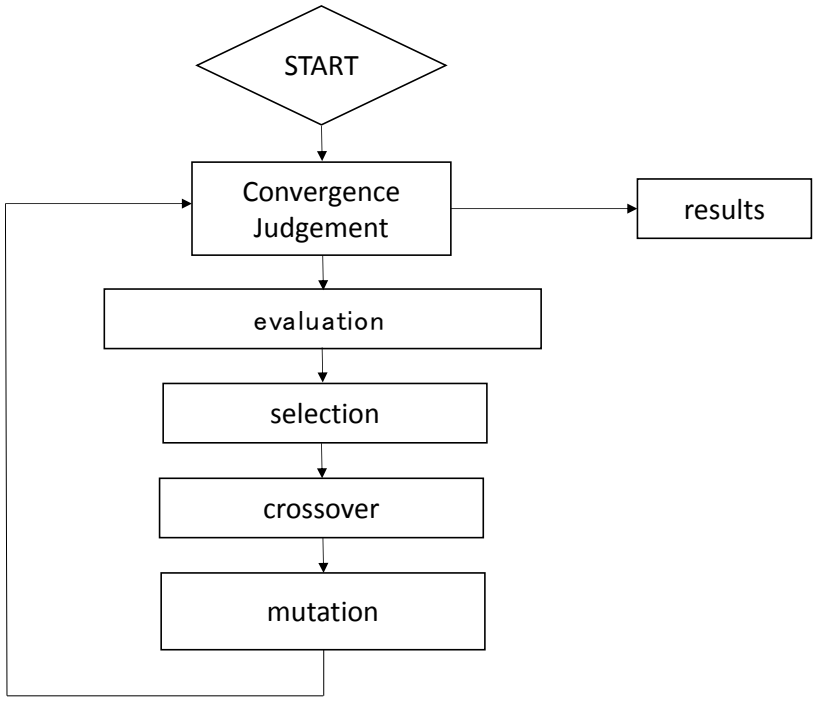

Fig. 2.8 process of typical genetic algorithm

As illustrated as Fig. 2.8, a typical process of GA can be described as a loop consisting of evaluation, selection, crossover, and mutation. At the end of every loop, the convergence of algorithm is judged, on which to decide if the algorithm should continue.

The steps in loop are explained as followings.

[1] Evaluation

For individuals who have not been evaluated, the objective functions of them are calculated. Depending on the requirements of problem and algorithm, the fitness of individual is determined by the objective functions and constraints of optimization problem.

[2] Selection

In order to generate new individuals in next generation, which is called as children in GA, individuals need to be selected to decide which individuals can be the parents, based on the fitness of them.

[3] Crossover

After the parents to generate children are selected, based on the genes of parents, the genes of children are decided from the crossover between the genes of parents.

[4] Mutation

In case of the population converging too fast, it is required that mutation happens on the genes of children from time to time according to determined probability. By this way, larger search space can be ensured.

[5] Convergence judgement

Usually, the convergence condition is set as an expected value of objective function, or a fixed number of maximum iterations. For the former, the algorithm will terminate when the objective functions of elite individuals or the average of population reach the expected values. While the evolution will continue until the iterations reach the limit, for the latter.

2.3.1.1 micro-GA

Generally, to ensure the performance of algorithm, the size of population in GA need to be large enough, which leads to more evaluation in each generation, and longer computation time for whole optimization. In some cases like FEM computation, fewer evaluation is preferred because every evaluation can cost long time. For this reason, with smaller population, micro-genetic algorithm (micro-GA) is used to settle with such situation [25]. Comparing to the general GA which usually has dozens or hundreds of individuals, the population for micro-GA is less than ten, making it much more time-saving.

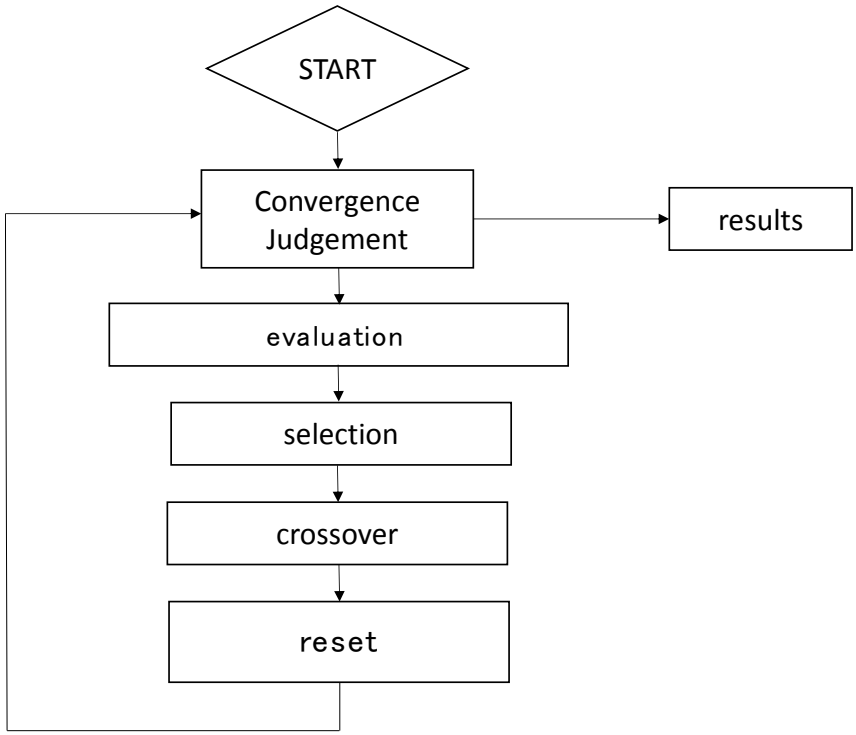

Fig. 2.9 process of micro-GA

The process of micro-GA is illustrated as Fig. 2.9, where the difference with typical GA is that there is no mutation in micro-GA but replaced by reset. As mentioned above, the population for micro-GA is usually far less than that for GA, which makes mutation is not effective enough to ensure the search space. Thus, in micro-GA, the individuals except for the elite one will be reset every couple of generations, by regenerating the genes of them randomly. The reset period needs to be decided in advance.

2.3.1.1 NSGA-II

In some cases, the optimization problems have multiple objective functions, in which the problem cannot be described as (2.5) anymore. The first way to solve such problem is converting multi-objective functions to single objective function as shown in (2.10).

$$min. \leftarrow f(\boldsymbol{v_i}) = \sum_{j=1}^{n} w_j f_j(\boldsymbol{v_i}) \tag{2.10}$$

where f_j and w_j are the j-th objective function and the weight coefficient for it. By this way,

the multi-objective optimization problem can be described as a single objective problem expressed by f, which is the weighted sum of all objective functions. However, this method requires the weighted coefficient to be determined in advance, which strongly depends on the experience of designer and may has large influence on the optimization result.

To deal with such concern, instead of using objective functions to evaluate individuals directly, Pareto front is introduced, which is shown as Fig. 2.10. It allows the designer to get rid of the decision of weight coefficients, and makes tradeoff relationships between objective functions clearer. In Fig. 2.10, the Pareto front is applied on a two objective optimization problem, where z_1 and z_2 are the objective functions, and F_1, F_2, F_3, F_4 are the frontiers described as different fitness. And the fitness of all individuals is calculated by non-dominated sorting algorithm, whose process is as followings.

Step 1: define $i = 1$

Step 2: set the fitness of all the individuals that don't dominate any other individual as i. (Dominate: has larger values for all objective functions)

Step 3: $i = i + 1$.

Step 4: delete all the individuals found in Step 2. If there is any individual remained, repeat from Step2, if not, finish.

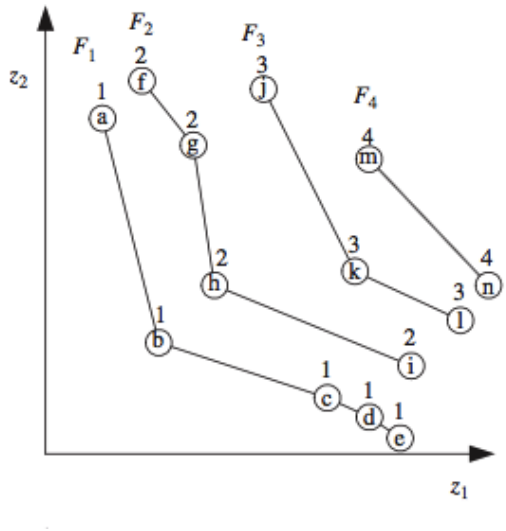

Fig. 2.10 Pareto front

By this way, the individuals can be evaluated by fitness, and the multi-objective optimization problem can be described as (2.11), without considering the decision of weight coefficients.

$$f(\boldsymbol{v_i}) = \begin{cases} f_1(\boldsymbol{v_i}) \rightarrow min. \\ \cdots \\ f_j(\boldsymbol{v_i}) \rightarrow min. \end{cases} \tag{2.11}$$

Based on the concept of Pareto front, Non-dominated Sorting Genetic Algorithm II (NSGA-II) is proposed for solving multi-objective optimization problem [26]. In addition, calculated as equation (2.12), crowded distance is introduced in NSGA-II to compare individuals with same fitness.

$$cd_k(I[i,k]) = \frac{f_k(I[i-1,k]) - f_k(I[i+1,k])}{f_k^{max} - f_k^{min}} \tag{2.12}$$

where f_k^{max} and f_k^{min} is the maximum (minimum) value for f_k among all the individuals in this generation. And the indices i and k are the sequence number of individuals and objective functions, while the individuals are sorted according to each objective function. Crowded distance is used to described how the individual is clustering with the others. During the optimization, for ensuring the diversity of individuals and the size of search space, the individuals with larger crowded distance are preferred in selection.

2.4 Single-objective optimization

In this section, two single-objective topology optimizations are going to be introduced. In both works, the coupling coefficient k, whose calculation is introduced in equation (2.1), is set as the objective function of optimization.

2.4.1 H-shape core

In first work, the magnetic core in WPT coupler with H-shape core is optimized using NGnet on/off method and micro-GA. As mentioned in section 2.1.1, coupler with H-shape core is proposed to improve the tolerance to lateral misalignment. The specific structure considered in this work is shown as Fig. 2.11.

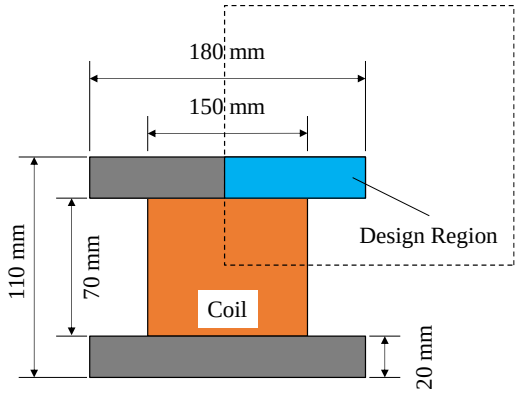

Fig. 2.11 Coupler with H-shaped core

where the orange and grey part represent the coil and magnetic core respectively. In order to save computation cost, only a quarter of the model is simulated and optimized in the FEM computation for evaluating individuals in micro-GA, while the rest in model is determined by symmetry. Other parameters of WPT system and coupler are listed in Table 2.1.

Table 2.1 Parameters of WPT system and coupler

Operating frequency	20 kHz
Current	1 A
Strand radius	0.15 mm
Number of strands	100
Number of turns	20
Transmission distance	40 mm

The optimization problem with the constraint in this work is written as (2.13).

$$F = k \rightarrow \max. \quad \text{sub. to } \Omega_M \leq \Omega_D/2 \tag{2.13}$$

where k, Ω_M, Ω_D denote the coupling coefficient, volume of magnetic core with optimized shape, and volume of design region, respectively. The volume constraint is introduced to obtain optimized design with higher k and smaller core – also lower cost of production – at same time.

Micro-GA is adopted to solve this optimization problem, and the parameters of it are listed in Table 2.2.

Table 2.2 micro-GA parameters

Population	5
End generation	350
Reset generation	5
Crossover	BLX-α [27]

A three-dimensional topology optimization is considered in this work by placing two layers of NGnet bases on the design region uniformly. In total, 112 bases with standard deviation of 5 mm are settled.

The optimization is implemented while the magnetic relative permeability is set as 10 and 100 respectively, to see the effectiveness for different material for magnetic core. A reference model as shown in Fig. 2.12 is simulated as well to give a comparison for the optimized results as shown in Fig. 2.13, while the magnetic flux of them is illustrated together.

The self-made FEM and micro-GA programs are made in C++, and the mesh generation for FEM computation is by commercial software JMAG. All the proposed works in this chapter are implemented with these programs and software.

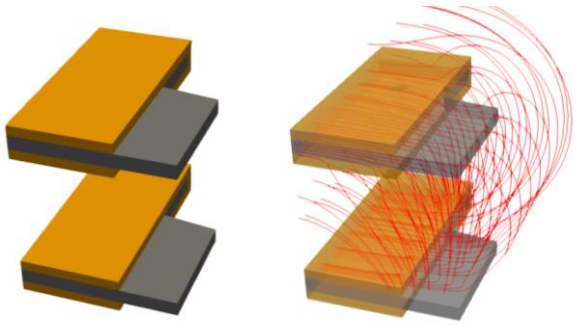

Fig. 2.12 Reference model (H-shaped core coupler)

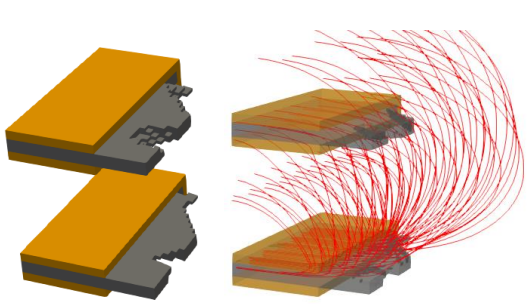

(a) Optimized core shapes ($\mu_r = 10$)

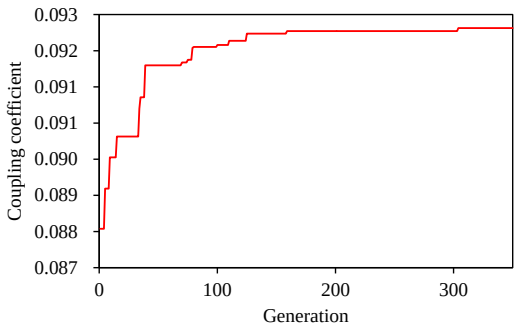

(b) Convergence history ($\mu_r = 10$)

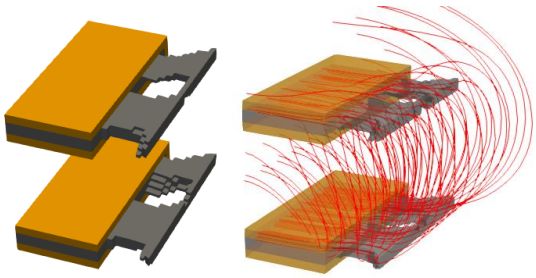

(c) Optimized core shapes ($\mu_r = 100$)

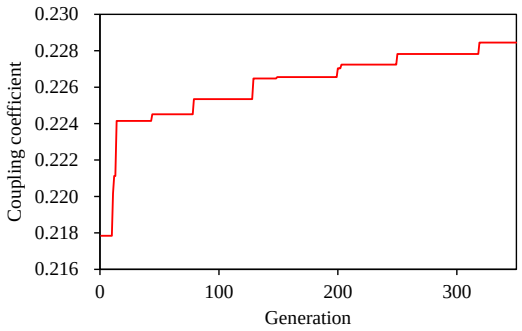

(d) Convergence history ($\mu_r = 100$)

Fig. 2.13 Optimized results (H-shaped core coupler)

Table 2.3 Comparison of optimized and reference model

	Optimized	Reference
$\mu_r = 10$	0.093	0.091
$\mu_r = 100$	0.228	0.215

The comparison between optimized and reference design is listed in Table 2.3. It shows that for both permeabilities the optimized models have higher coupling coefficient than the reference model, which means better transfer efficiency of WPT. The coupled phenomenon can be seen in the magnetic flux distribution, more fluxes are coupled to the receiving coupler in the optimized model with higher permeability.

The convergence histories of two optimizations are shown as Fig. 2.13 (b) and (d), where obvious increase can be seen on the objective function – k of WPT. Although the convergence condition of evolution was set in 350 generation based on designer's experience, it seems like there is still potential of optimization for the second optimization according to Fig. 2.13 (d).

2.4.2 DD-shaped coil

Introduced in section 2.1.1 as well, coupler with DD-shaped coil is another design proposed for improve anti-misalignment performance of WPT system. In this section, two works considering different designs are introduced, and both of them are going to be optimized using the method discussed above.

2.4.2.1 Typical structure

Firstly, a typical structure of coupler with DD-coil is shown in Fig. 2.14.

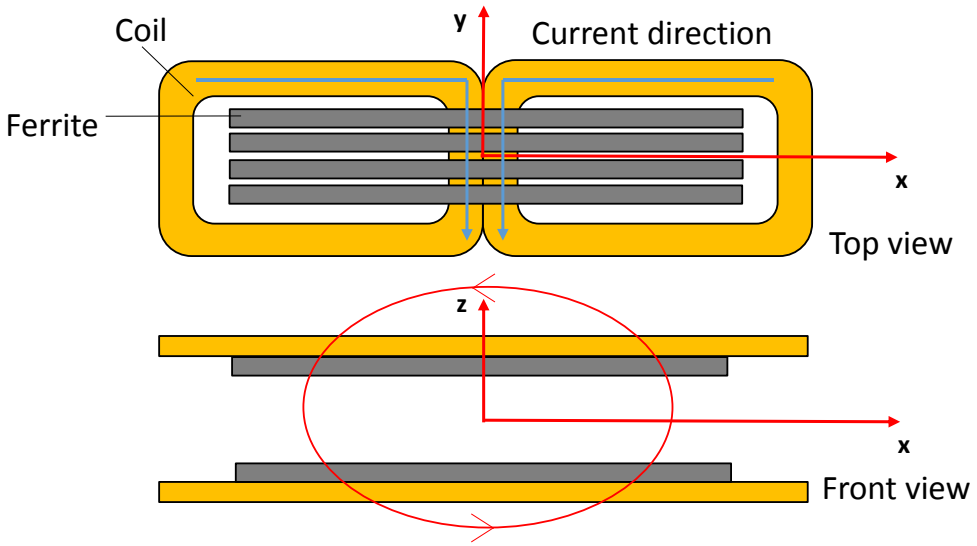

Fig. 2.14 Coupler with DD-coil

As denoted in Fig. 2.14, the current directions of two D-shaped coil are opposite, which makes the magnetic flux of the coupler is like what illustrated in the below. The flux pass through the receiving coupler along x-direction is the reason why DD-coil has better anti-misalignment performance than traditional circular coil.

The simulation model is shown in Fig. 2.15. Similar to the work in previous section, only a quarter of the model is optimized and computed in program for saving computation cost. In this work, different amounts of Gaussian bases of 200, 112, and 348 have been considered to see the influence of it on optimization results.

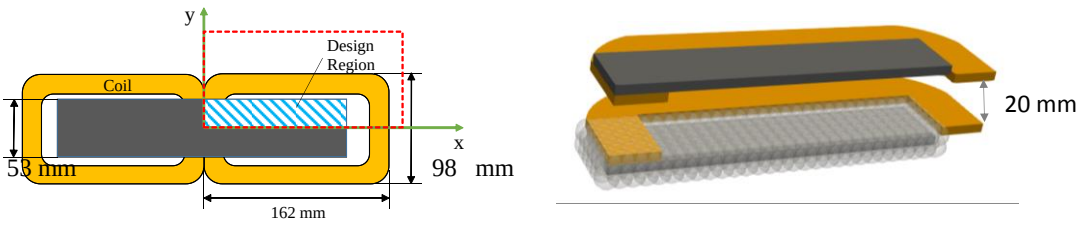

(a) Size diagram (b) NGnet placement

Fig. 2.15 simulation model (DD-coil coupler)

Other parameters of the model are listed in the table below. The optimization problem of this work is same as (2.13) – maximizing the coupling coefficient with a constraint that the designed

shape should have a volume smaller than half of the total volume of design region. Micro-GA is adopted to solve this optimization problem, while the parameters of it are same with Table 2.2.

Table 2.4 Parameters of WPT system and coupler

Turns of coil	20
Transmission distance	20 mm
Frequency	20 kHz
Current	1 A

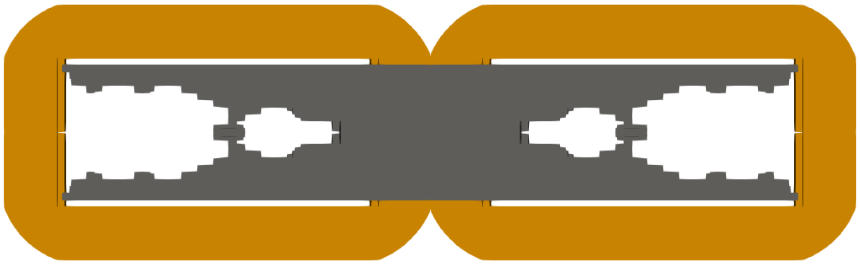

(a) Gaussians = 112

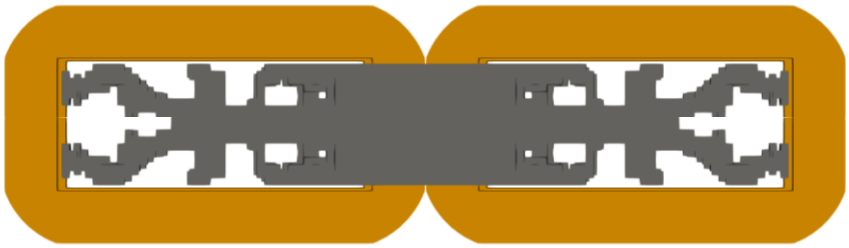

(b) Gaussians = 200

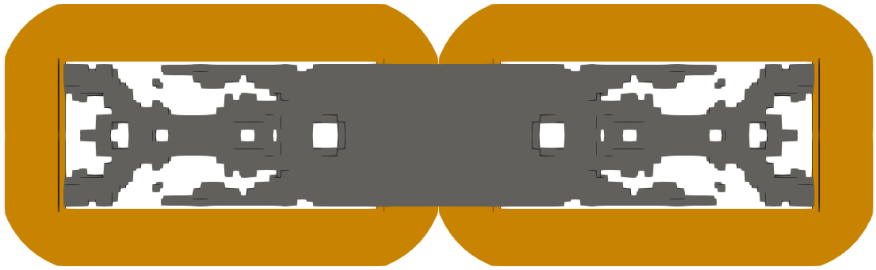

(c) Gaussians = 348

Fig. 2.16 Optimized results (DD-coil coupler)

Table 2.5 Comparison results (DD-coil coupler)

	k	volume
112 Gaussians	0.6318	$\leq \Omega_D/2$
200 Gaussians	0.6308	$\leq \Omega_D/2$
348 Gaussians	0.6342	$\leq \Omega_D/2$
Reference model	0.6271	$= 0.53\Omega_D$

Finally, the representative results after 350 generation revolution under each NGnet setup are shown in Fig. 2.16, and the comparison between them and reference model which is illustrated as Fig. 2.14 is given in Table 2.5. It shows that all the NGnet setups finally obtained optimized results with higher k than reference model, and lower volume of magnetic core. In the three optimized results, that with 348 Gaussian bases has the highest k.

Because micro-GA is an algorithm with relatively narrow search space, usually the optimization needs to be performed several times with different random initial individuals to ensure big enough search space can be covered in the optimizations, so did the works in this section. The average results of optimizations with three NGnet setups are summarized in Table 2.6. It can be seen that the more Gaussian bases are placed, the higher average k optimizations got, which demonstrates that the potential of optimization using NGnet on/off method is in proportion to the number of placed Gaussian bases. Whereas, more Gaussian bases means higher complexity of optimization problem. It asks the designer to balance these two issues.

Table 2.6 Average results of optimizations

	k
112 Gaussians	0.6296
200 Gaussians	0.6304
348 Gaussians	0.6333

2.4.2.2 Leakage reducing structure

Above the basic design introduced in previous section, a modified design for reducing leakage

magnetic flux was proposed in [28], which is showed in Fig. 2.17. The structure and topology of coils is same as the typical type, which means that the basic theory is still same, while the magnetic core is extended outside the coil, covering the coil slightly along the z direction. This design can gather more flux in the outside of coils, preventing them from throwing far away. By reducing leakage magnetic flux, both the coupling between couplers and electromagnetic radiation of WPT system can be improved.

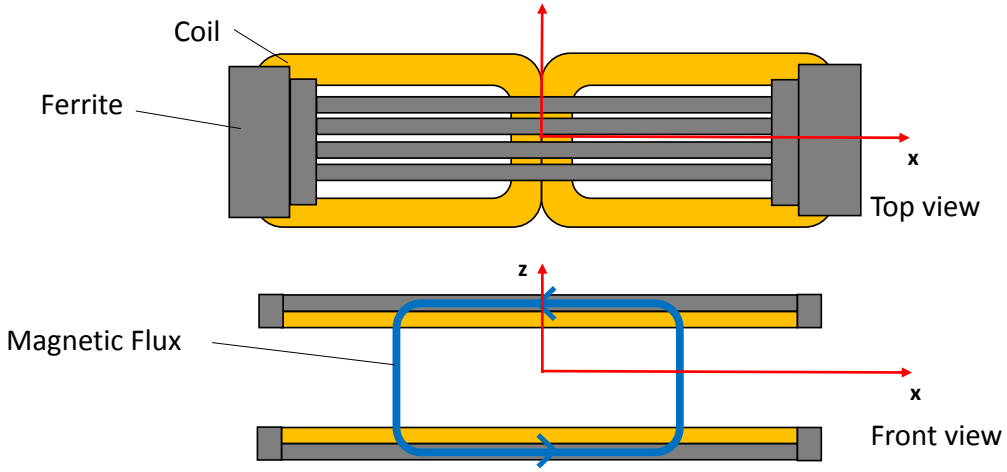

Fig. 2.17 Leakage reducing design of DD-coil

Based on this design, topology optimization is performed. The general size and parameters in simulation model are same with what is described in previous section. As written in (2.14), though the objective function remains same, the constraint is changed to requiring the optimized shape has less volume than a third of volume of design region. The NGnet placement is shown as Fig. 2.18, where 182 Gaussians are placed in two layers. Moreover, gap between transmitter and receiver of 20 and 40 mm are considered respectively, and the results are shown in Fig. 2.19, while the comparison between them and the reference model shown as Fig. 2.17 is given in Table 2.7.

$$F = k \to \max. \quad \text{sub. to } \Omega_M \leq \Omega_D/3 \tag{2.14}$$

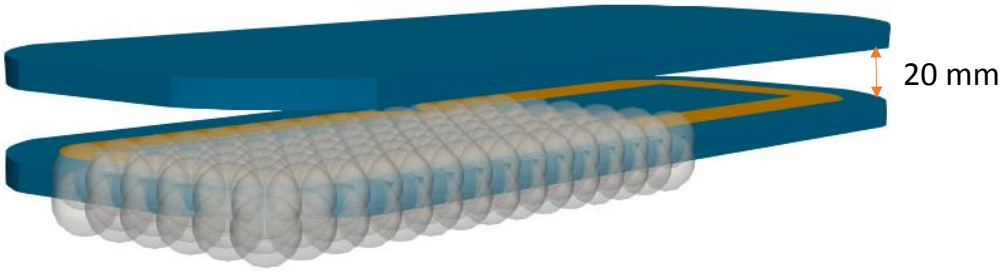

Fig. 2.18 NGnet placement

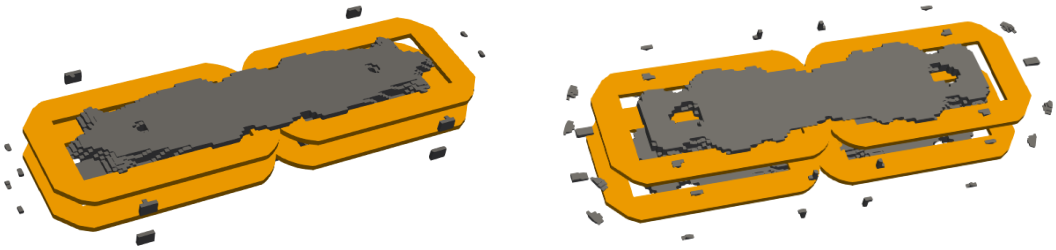

(a) Gap = 20 mm (b) Gap = 40 mm

Fig. 2.19 optimized model

Table 2.7 Comparison results

		k	k (without floating pieces)
Gap = 20 mm	Optimized model	0.7182	0.7183
	Reference model	0.6741	
Gap = 40 mm	Optimized model	0.4566	0.4529
	Reference model	0.4173	

It shows that in both case of gap, the optimized models have higher k than reference model, which proves the effectiveness of the optimization method. Remarkably, there are some floating tiny pieces isolated from the main core. Obviously, those tiny pieces cannot be produced in practice, so the optimized models are evaluated with the pieces are eliminated to see if the performance is still good. The k of the optimized models without floating pieces are listed in the right of Table 2.7. It can be seen that their coupling coefficients don't change too much after

eliminating the pieces, demonstrating the effectiveness of the main part of optimized designs.

Moreover, there is little core remained near the outside of coil in both optimized models, which seems contradictory with what is discussed in [28]. There are two possible reasons for it.

Firstly, the transfer distance considered in this work is relatively short compared to the size of coils. In this case, the main flux to transfer the energy is majorly concentrated around the center of couplers. Thus, the optimizations tend to gather magnetic core near the center to enhance the main flux, instead of preventing magnetic flux from leakage.

Secondly, the effect of outside magnetic core on reducing leakage flux does not necessarily have obvious improvement of coupling coefficient. Even though the leakage flux can be gathered towards coil due to the existence of outside core, it cannot be ensured if and how much flux will be coupled to the receiving coil. That is why the optimization of coupling coefficient tends to approach designs without outside core. But if the safety of WPT system, which can be considered as the leakage magnetic field far away from the WPT system, needs to be optimized at same time, the decrease of leakage flux will be important even though not coupled to the receiver. In next section, several works of multi-objective optimization for coupling coefficient and leakage magnetic field together will be introduced.

2.5 Multi-objective optimization

As mentioned in section 2.1, the safety is also an important issue of WPT research and development. As ruled in standards [[17], [18], [29]], for frequency ranging from 3 kHz to 10 MHz, the magnetic flux exposure to human bodies should be limited up to 27 μT for general public exposure, and 100 μT for occupational exposure. For this reason, optimizations considering transfer efficiency and leakage filed simultaneously are called for improving WPT device

In this section, multi-objective optimizations are performed on couplers with circular and DD

coil. The increase of coupling coefficient and the reduction of leakage flux are set as the optimization objectives.

2.5.1 Circular coil

As mentioned in section 2.1.1, circle is a representative topology of coil design in WPT coupler. It has advantages like ease of manufacturing and magnetic flux pattern. In [30], like what is done to coupler with DD-coil in [28], the magnetic core of circular coupler is optimized using PSO, and the results show that a structure of magnetic core covering the coil in some extent helps increasing coupling effect and decrease leakage magnetic flux.

Based on that, in this section, multi-objective topology optimization is performed on the magnetic core shape to find designs with better performances. Prepared to be compared with optimized results, the reference model is constructed as Fig. 2.20. The bar-shaped ferrite has same structure as shown in Fig. 2.21, where the ferrite beneath the coil is thinner, forming the covering structure. The bar-shaped topology in reference model is referring to the optimized results reported in [31].

The diagram of design model is shown in Fig. 2.21, together with the arrangement of Gaussian bases. Similarly, the optimization and simulation are only performed in a quarter of whole model to save computation cost. An evaluation region is placed outside the coupler, in which the maximum magnetic flux density is used to represent the leakage magnetic field. A 2D topology optimization is applied on the magnetic core, by placing 69 Gaussians on the design region.

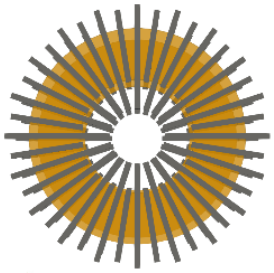

Fig. 2.20 Circular coil

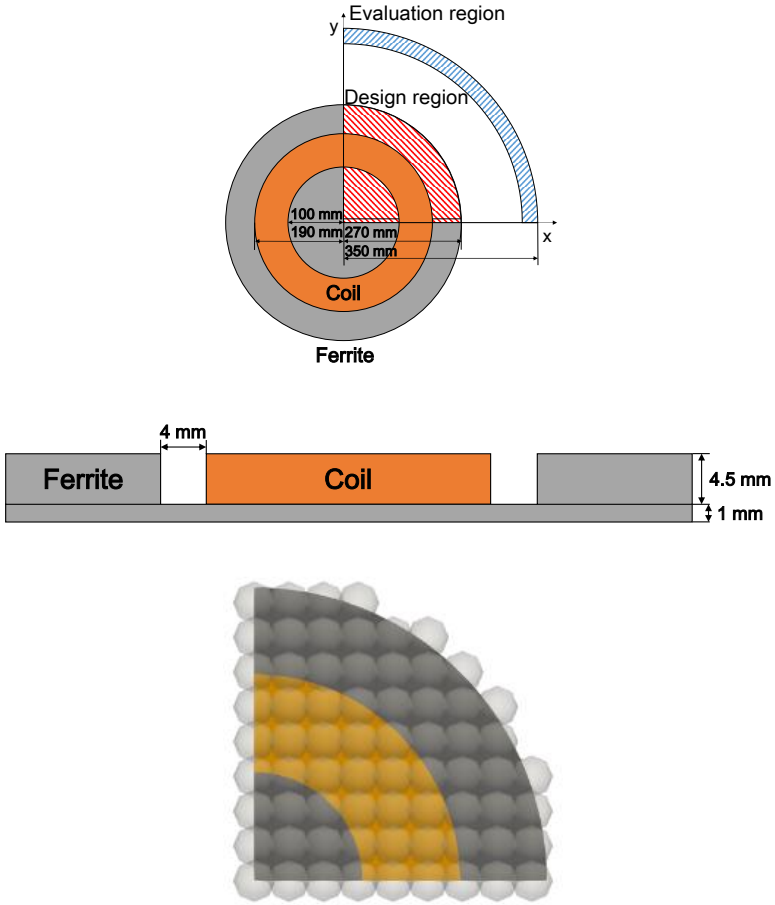

Fig. 2.21 Diagram and arrangement of Gaussians (circular) ©2020 IOS Press

The optimization problem is described as (2.15). The increase of k and decrease of maximum flux density in evaluation region are chased together, while the constraint requires the volume of optimized shapes $\Omega_{opt.}$ to be lower than c times volume of reference shape $\Omega_{Ref.}$. c is a predetermined constant, which is set as 1.0 and 1.1. The optimizations are performed with two values of c respectively.

$$F = \begin{cases} k \to \max. \\ B_{\max} \to \min. \end{cases}, \qquad \text{sub. to } \Omega_{opt.} \leq c * \Omega_{Ref.} \tag{2.15}$$

NSGA-II is adopted to solve this multi-objective optimization problem. The parameters of WPT system and NSGA-II are listed in Table.

Table 2.8 Parameters of WPT system and NSGA-II ©2020 IOS Press

I (abs)	23 A	Parent population	120
Air gap	100 mm	Child population	120
frequency	20 kHz	End generation	150
Turns of coil	20	Crossover probability	95%
Ferrite μ_r	1000	Mutation probability	5%

Finally, the Pareto front of optimizations with c of 1.0 and 1.1 are plotted together with the point of reference model in Fig. 2.22.

By relaxing the constraint condition, the Pareto front shows advance towards optimization direction. And both the optimizations with two constraints obtained optimized results which have lower leakage flux density than the reference model, while none of them can get results with higher coupling coefficient. Two optimized designs with their magnetic flux pattern shown in Fig. 2.23, together with the reference model.

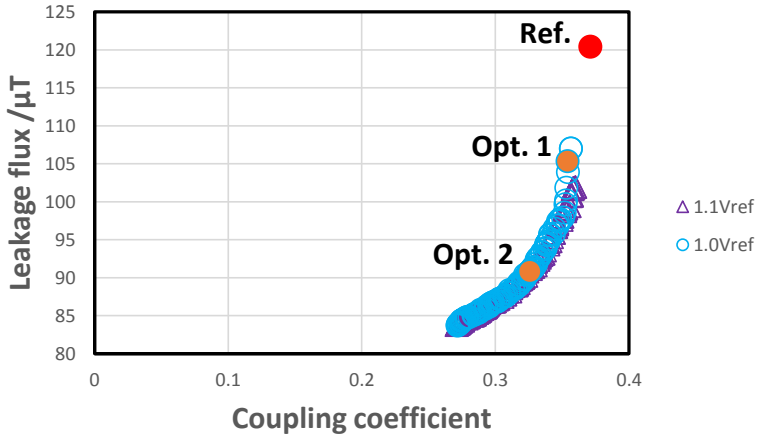

Fig. 2.22 Pareto front of optimization for circular coupler ©2020 IOS Press

(a) Reference model ($k = 37.1\%, B = 120.4$ μT)

(b) Optimized model 1 ($k = 35.4\%, B = 105.3$ μT)

(a) Optimized model 2 ($k = 32.6\%, B = 90.8$ μT)

Fig. 2.23 Reference model and optimized models (Circular) ©2020 IOS Press

2.5.2 DD coil

Similar optimizations are performed on magnetic core of DD coupler, whose structure is shown as Fig. 2.24. The evaluation region is placed 105 mm far away from the design region. The optimization problem is same with (2.15), performed two times with different value of constant c. The Parameters of WPT system and NSGA-II are same with previous work as well, as summarized in Table 2.8. For NGnet, 126 Gaussian bases are placed uniformly.

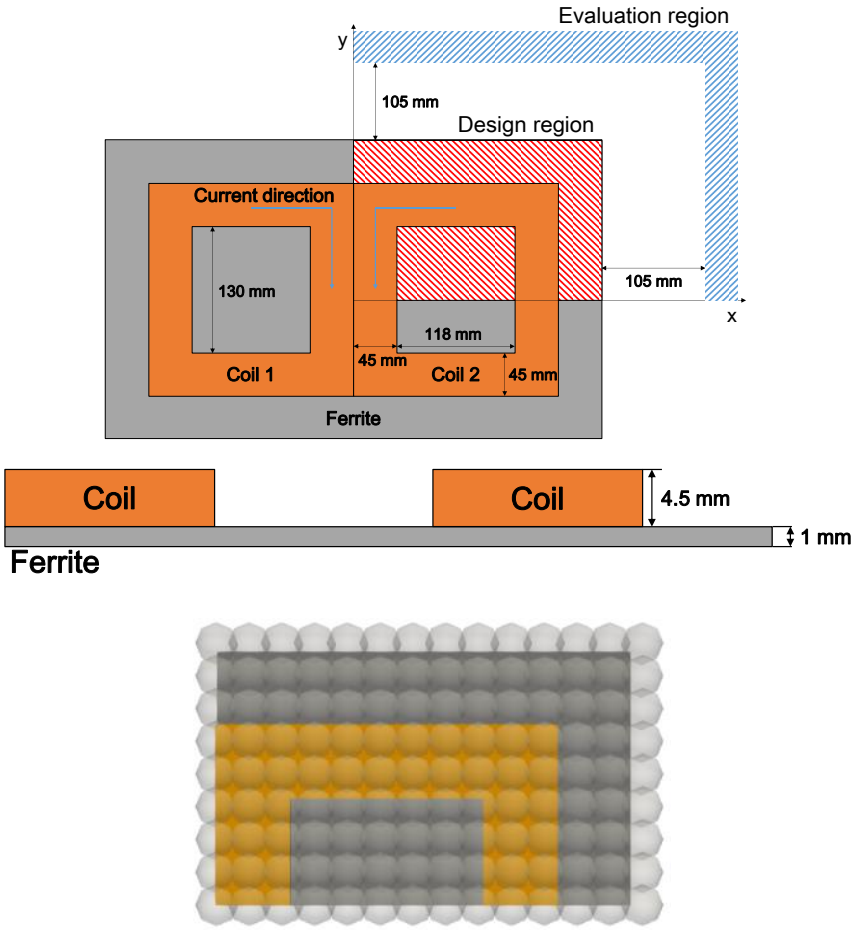

Fig. 2.24 Diagram and arrangement of Gaussians (DD) ©2020 IOS Press

The Pareto front obtained by the optimizations are shown in Fig. 2.25, while two representative optimized results and the reference model are illustrated in Fig. 2.26. A similar result that all the optimized results got lower leakage flux but few of them have higher coupling coefficient than the reference model. In Fig. 2.26 (b), an optimized design with better performances of both two objective functions is shown. It has a somehow bar-shaped ferrite but with less and thicker bar shape.

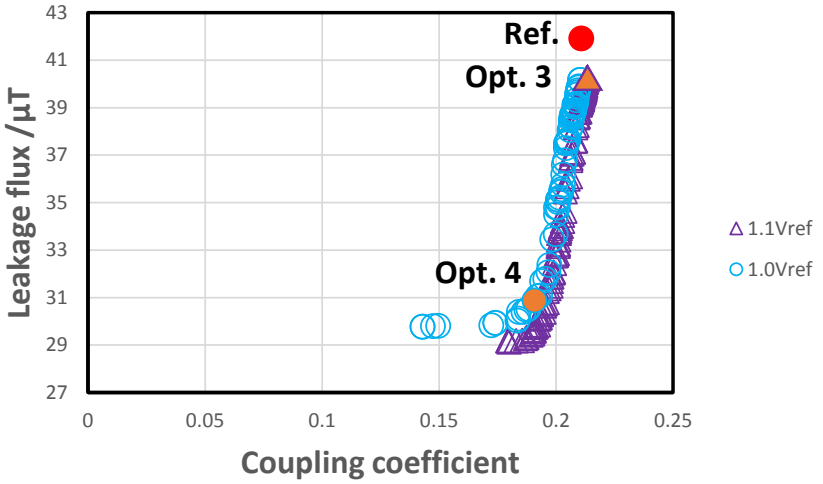

Fig. 2.25 Pareto front of optimization for DD coupler ©2020 IOS Press

(a) Reference model ($k = 21.1\%, B = 42.0$ μT)

(b) Optmized model 3 ($k = 21.3\%, B = 40.3$ μT)

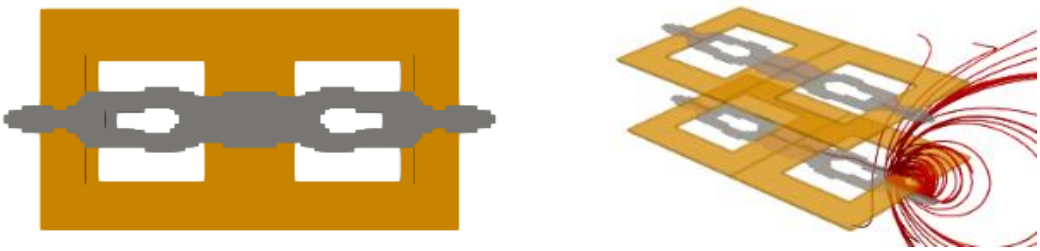

(c) Optmized model 4 ($k = 19.1\%, B = 30.9$ μT)

Fig. 2.26 Reference model and optimized models (DD) ©2020 IOS Press

2.6 Conclusion

In this chapter, the backgrounds of WPT, topology optimization, and optimization algorithm have been introduced. Especially, the calculation in WPT system, NGnet on/off method, and genetic algorithm used in the proposed works are explained in detail. Based on these methods, the magnetic cores in different topologies of WPT coupler are optimized to obtain better performances with less ferrite used.

As a result, several novel shapes of magnetic cores have been gotten and discussed in this chapter. It shows that the proposed method can obtain novel designs with better performances under predetermined constraints. Although the optimized shapes are sometimes hard to be produced in practice consistently, they can provide reference for the practical production by summarizing the relationship between the shape patterns and the performances.

Chapter 3 Optimizations of transmitting coil in WPT coupler

As discussed in previous chapters, the topology of transmitting coil has a fundamental influence on the system performances, for it determining many important properties of WPT like magnetic flux pattern. And as we have mentioned before, many researches have been proposed to improve WPT by designing new coil topology, like DD-coil [11] and H-shaped core [12]. Both of them try to improve the anti-misalignment, which is one of the most common factors influencing the performances of WPT system, by designing the coil topology to make the magnetic flux through receiving coil have longer span over the misalignment direction.

Except for the coil topology design, multi-coils have been discussed a lot to improve anti-misalignment performance as well. As summarized in [32], in recent years, many researches of WPT coil design have been proposed using multi coils and three-phase electric power. Without designing new complicated coil shape, anti-misalignment performance is ensured by combing individual input control with multi-coils. In [33], a tripolar pad including three coils somehow overlapping each other is proposed, with the input controls of them are optimized to make the WPT system has better anti-misalignment performance for all the misalignment directions. And in [34], based on target field method, the topology of multi-coils is optimized considering transfer efficiency and leakage magnetic flux at same time.

Having a wild application on the design of magnetic resonance imaging coil [34][35], [36], target field method is going to be used here to optimize transmitting coil design. In target field method, usually the relationship between generated magnetic field and current density in coil is built by Bio-Savart law [37]. And the current density in coils can be easily computed when the coil shape

is described by stream function. The specific calculating processes will be introduced later in this chapter.

In this chapter, we aim to obtain optimized multi-layers coil design by using target field method and NGnet method, considering transfer efficiency and leakage magnetic field simultaneously under different misalignment conditions. Assuming the exact misalignment distance is known by position prediction technique, which will be discussed and realized in later chapter, a simple control strategy for input current is designed and applied on the multi-layers coil. The optimization problem is solved by multi-objective Covariance Matrix Adaptation Evolution Strategy (MO-CMA-ES) [38]. Finally, a representative optimized result is picked and compared with the reference model. It shows that the optimized one has close performance when no misalignment, but better anti-misalignment performance.

3.1 Multi-layers coil and control-strategy

With reference to WPT1/Z1 standard [17], a resonance WPT system operating at 85 kHz with transfer distance of 0.1m is considered in this work. The scheme of the system is shown in Fig. 3.1 (a), where the primary side of WPT system consists of three coils and a ferrite layer with its relative permeability set as 2300. The design region of three-layer coils overlaps each other, with a size of 0.6 * 0.6m. From top to bottom, left, right, and middle coil are placed, while the design of receiving coil is fixed. Treating the coils as litz wire, the thickness of coil layer is set as 4.5mm, though the field computation is implemented only in two-dimension space, the thickness is considered as the gap between coil layers. This scheme is determined according to what is specified in [17].

The equivalent circuit of this multi-layer coil system is illustrated as Fig. 3.1 (b), where R_{pi}, L_{pi}, denote the equivalent resistance, self-inductance of the coils, while C_{pi} represent the capacitor attached to adjust resonance frequency, and M_i is the mutual-inductance between

receiving coil and each transmitting coil. The mutual-inductances between transmitting coils are ignored for simplification. Three individual input current sources I_i are set for the three transmitting coils. A $20\,\Omega$ resistance is attached on the receiver coil as system load. The parameters of transmitting coils are decided by calculation which will be introduced later, and the parameters of receiving coil are calculated according to the pre-determined design, and remain unchanged during the optimizations. It should be noted that, both transmitting and receiving side of the system are assumed to work in resonance all the time, for simplification.

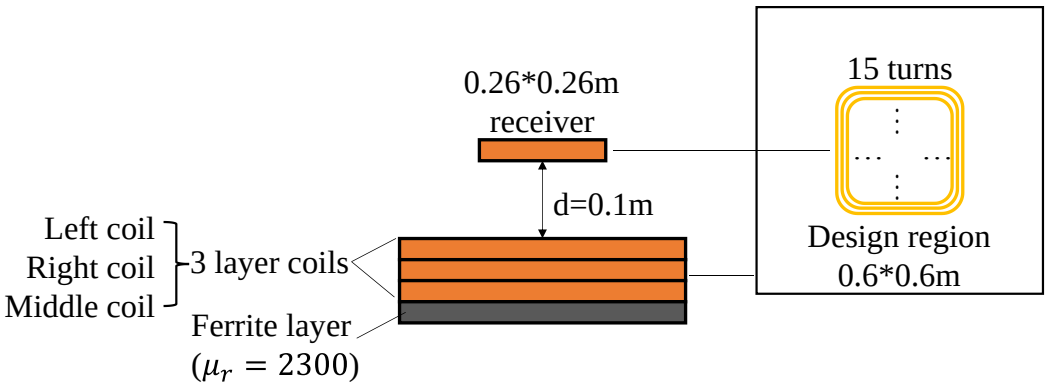

(a) Multi-layers coil system

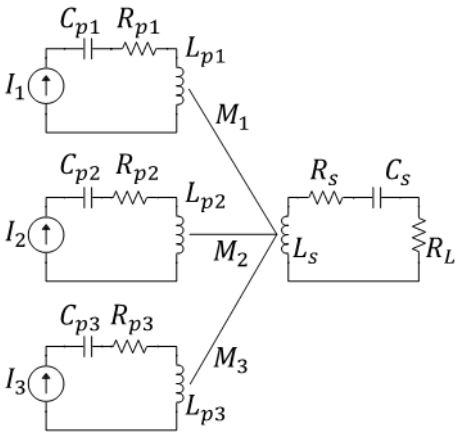

(b) Equivalent circuit

Fig. 3.1 WPT system

Based on this equivalent circuit, the output power P_{out} on the load resistor R_L can be calculated as following equation.

$$P_{out} = \left(\frac{\sum_{i=3}^{3} j\omega M_i I_i}{R_s + R_L}\right)^2 \cdot R_L \tag{3.1}$$

R_s - the equivalent resistance of receiving coil - is calculated by multiplying unit resistance of litz wire [39] and the length of coils, which is pre-determined. Because the system is assumed to be in resonance, the system efficiency can be simply expressed by magnetic efficiency, calculated as (3.2), according to [40].

$$\eta_{mag} = \frac{P_{out}}{P_{in}} = \frac{P_{out}}{\sum_{i=3}^{3} R_{pi} I_i^2} \tag{3.2}$$

A simple control-strategy for the three transmitting coils is designed, as illustrated in Fig. 3.2. With an assumption that only one misalignment direction is considered, and the exact misalignment distance is known, a multiplier c_i is defined for each coil, which are complex number in order to realize magnitude and phase control together. However, we take the RMS value of the performances and the quantities as the objective functions in optimization. Additionally, we assume that left coil is totally symmetrical with right coil, so that the shapes and c_i of them are symmetric as well. The input current of each coil will be multiplied with c_i to realize the misalignment-based control.

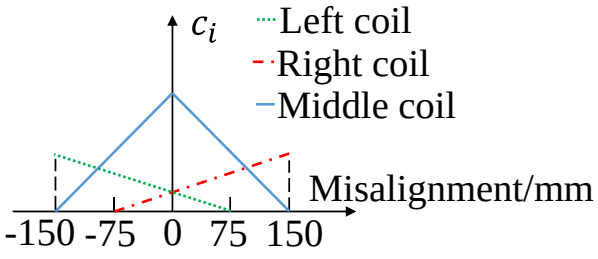

Fig. 3.2 Multi-layer coils control-strategy

3.2 Target field method

In this work, the field computation is implemented within static magnetic field. And the

relationship between magnetic flux density and current density is described as the following, according to Bio-Savart law.

$$\boldsymbol{B}(\boldsymbol{r}) = \frac{\mu}{4\pi}\int_{S} \boldsymbol{J} \times \frac{\boldsymbol{r}'}{|\boldsymbol{r}'|^3} dS \tag{3.3}$$

where μ is the permeability, and $\boldsymbol{J}$, $\boldsymbol{r}'$ are the current density and the displacement vector from dS to observation point r, while dS is the space element in design regions of three transfer coils.

In target field method, stream function $\boldsymbol{S}$ is introduced to describe the current density $\boldsymbol{J}$ and the current value I of coil, as written in following equations.

$$\boldsymbol{J} = \nabla \times \boldsymbol{S} \tag{3.4}$$

$$I = \frac{(S_{max} - S_{min})}{N} \tag{3.5}$$

where S_{max} and S_{min} are the maximum and minimum value of the stream function $\boldsymbol{S}$, while N is the number of turns of coil, which is pre-determined as 20 during the optimization. It needs to be mentioned that for stream function $\boldsymbol{S}$, only the component vertical to coil layer is considered in the calculation. And the coil shape can be obtained by drawing the contour line of stream function, which is realized by using library matplotlib [41]. In addition, we impose the stream function to be 0 along the edge of design region for purpose of acquiring closed coil shape.

Besides, the magnetization current $\boldsymbol{J_m}$ within ferrite layer is considered, whose calculation is described as the followings.

$$\boldsymbol{J_m} = \nabla \times (\chi_m \boldsymbol{H_i}), i = 1,2,3 \tag{3.6}$$

$$\chi_m = \mu_r - 1 \tag{3.7}$$

where $\boldsymbol{H_i}$ and $\boldsymbol{\chi_m}$ **a**e the magnetic field generated from each transmitting coil, and the magnetic susceptibility of the ferrite. In this way, the contributions from magnetization current to generated magnetic field within the space of receiving coil can be calculated, using Bio-Savart law as well.

Finally, the mutual inductances can be obtained, using equation (3.8).

$$M_i = \frac{\sum_{i=1}^{3} \int_S B_i \, dS}{I_i}, i = 1,2,3 \tag{3.8}$$

where B_i denote the flux density contributed by the current density of i-th coil and the magnetization current generated by i-th coil. And I_i represents the current of i-th coil, which is calculated by (3.5).

So far, the magnetic efficiency η_{mag} and output power P_{out} can be calculated from filed computation.

3.3 NGnet method

In this work, NGnet method is used to express and control stream function by individual variables. The calculation process of NGnet is referred to section 2.2.1. To reduce the complexity of the optimization problem, like what we did to the control strategy, symmetry condition is applied on the NGnet setting for three design regions. As shown in Fig. 3.3, for left and right coil, the Gaussian bases are placed over the half of whole region, and mirror symmetry is constrained for them, while Gaussian bases are deployed only in a quarter of design region for middle coil, and the rest space is expressed by rotational symmetry. In this way, the number of variables for NGnet is reduced to 24 in total.

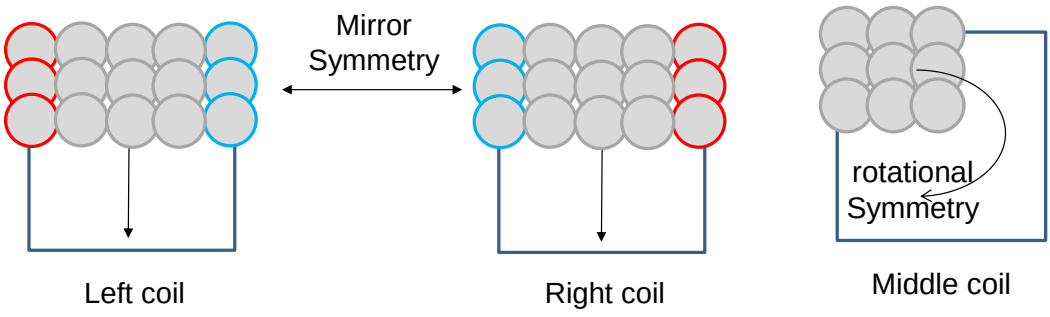

(a) Left and right coil (b) Middle coil

Fig. 3.3 NGnet setting for coils

3.4 Optimization setting

In this work, we want to optimize the coil design considering transfer efficiency and leakage magnetic field under misalignment conditions. The objective functions of this multi-objective optimization are summarized as following:

$$F = \begin{cases} \max\left(P_{out,j} - P_{tar}\right) \rightarrow min. \\ \min\left(\eta_{mag,j}\right) \rightarrow max. \\ \max(B_{leak,j)} \rightarrow min. \end{cases} \quad ,j = 1,2,\dots,5 \tag{3.9}$$

where j denotes the number of cases, and P_{tar} is the target output power which is set as 2500W, while B_{leak} is the leakage flux density in observation region. To sum up, the magnetic efficiency is required to be maximized, and the leakage flux density needs to be minimized, under all misalignment cases, while the output power is supposed to maintain in a fixed value as a constraint of optimization.

As illustrated in Fig. 3.2, totally 5 misalignment cases are considered, with a misalignment distance range from -150 to 150 mm, which is about two times of the maximum misalignment required to be considered, as specified in [17]. According to [17] as well, the observation area of leakage magnetic field is determined as shown in Fig. 3.4. With length of 0.1m along z direction, two observation area on y-z space are placed by the two sides of car. The magnetic flux density in the areas is calculated in each misalignment case to get the maximum value, which is used in the optimization and expected to be less than 27μT, as stipulated in [29].

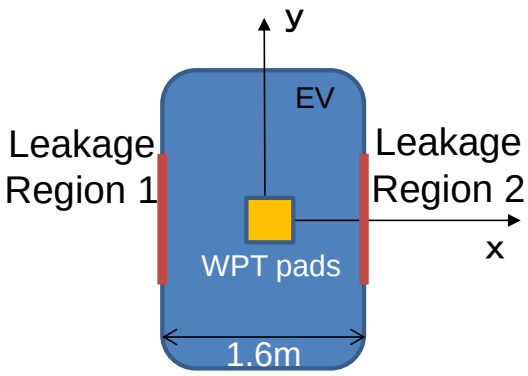

Fig. 3.4 Observation area of leakage magnetic field

Totally, there are 28 variables in the optimization, including 24 weights of NGnet and the others for expressing multipliers c_i. MO-CMA-ES is used as the algorithm for the optimization, and the parameters of it are listed in Table 3.1. All the program in this work is constructed in Python, while MO-CMA-ES is deployed using library DEAP [42].

Table 3.1 Parameters of MO-CMA-ES

Parent population	10
Child population	15
End generation	1000
Sigma	5

To sum up, the calculation process in every evaluation during the optimization is illustrated in Fig. 3.5, where the quantities colored as red are used to get calculate objective function subsequently.

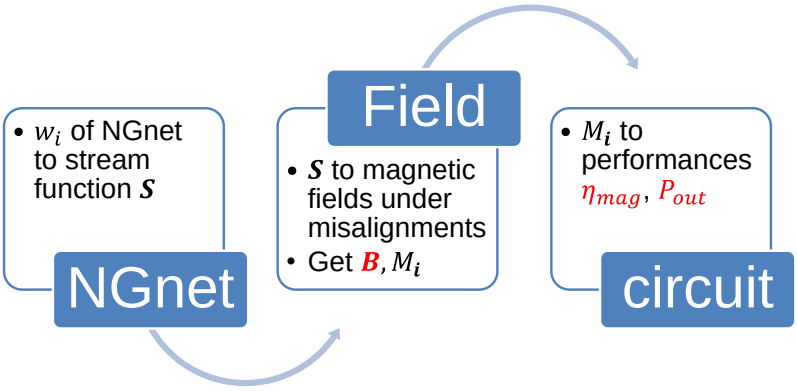

Fig. 3.5 Calculation process

3.5 Optimization result

A representative shape among the final optimization results is picked and shown in Fig. 3.6, where the symmetry of themselves and between left and right coil can be seen. To give a comparison with the optimized designs, a simple reference model is prepared as shown in Fig. 3.7. It is assumed that the reference model has three layers coil with same shape, and the input current of them is same as well, with an equal magnitude of the input current of middle coil in optimized model.

In Fig. 3.7 (a) and (c), it shows that the center of coil obviously moves to towards its responsible misalignment direction. And the middle coil has two symmetric centers placed along the misalignment directions.

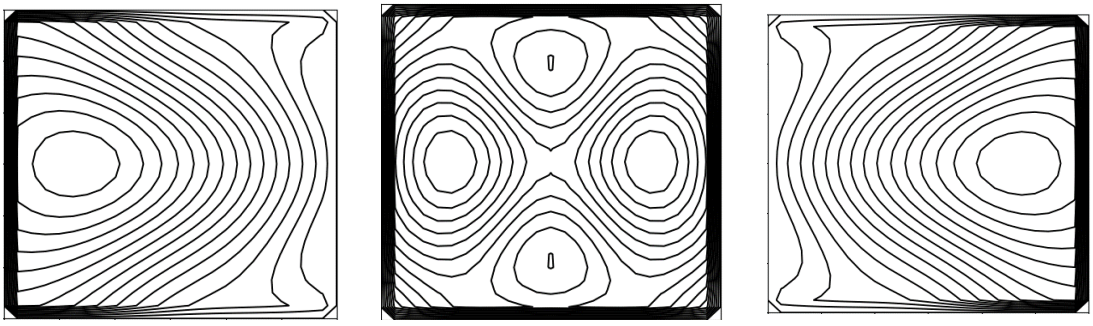

(a) Left coil (b) Middle coil (c) Right coil

Fig. 3.6 Optimized coil designs

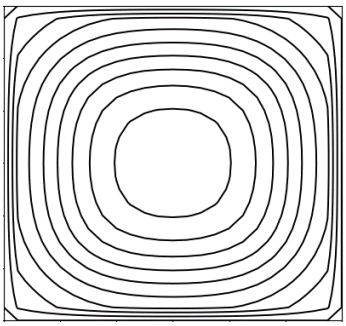

Fig. 3.7 Reference coil design

The performances of optimized and reference model under each misalignment case are compared and summarized in Table 3.2. It shows that the optimized one performs closely to the reference one when no misalignment, but has better anti-misalignment performance. When misalignment distance increase, all the three performances – output power, magnetic efficiency, maximum leakage flux density – of reference model degrade obviously. But the performances of optimized model don't decrease so much relatively, of which P_{out}, η_{mag}, $\max(B_{leak})$ can maintain in over 80%, over 2000W, and less than 40μT in all the cases. In addition, the reason why optimized model performs best under $\pm$75mm is considered that left/right coil and middle coil work together in this case because of the control strategy. It suggests that there may be room for improvement if better control strategy is adopted. Although P_{out} and η_{mag} are not bad, the maximum leakage flux density seems hard to be less than 27μT, which is the limitation specified

in [29].

Table 3.2 Performances comparison (optimized model / reference model)

Misalignment/mm	-150	-75	0	75	150
P_{out} / W	2496 / 1806	2244 / 2633	2813 / 2901	2197 / 2633	2812 / 1806
η_{mag} / %	82.2 / 75.9	86.3 / 81.9	83.3 / 83.2	86.0 / 81.9	83.8 / 75.9
max(B_{leak}) / μT	30.9 / 54.9	30.3 / 37.9	37.3 / 27.4	30.3 / 37.9	30.9 / 54.9

3.6 Conclusion

In this work, an optimization of WPT transmitting shape is proposed. Considering a multi-layer coil system with a simple control strategy for them, the designs of each layer coil is optimized using target field method. As a result, the representative optimization model shows better anti-misalignment performance on magnetic efficiency, output power and leakage flux density. However, the leakage flux density failed to be less than the limitation. It is considered that the control strategy of multi-coils can be improved further, to make the performances better.

Chapter 4 Metal object detection and position prediction in WPT system

As discussed in previous chapters, safety is an important issue of researches and developments of WPT. However, in the works introduced above, only the leakage magnetic field is considered for the safety issue, while there is another potential threat to the safety of WPT system. As discussed in [[17], [18], [43]], the existence of foreign object must be involved in the consideration of WPT system safety.

The possible foreign object in WPT system can be roughly divided into two types. Metallic object and living object. As for the former, metal can, flip, key are some typical objects that probably invade into WPT system. In the scenarios like charging station of EV, the magnetic field between the couplers is usually strong, which will generate eddy current inside the metal object, making the temperature of the object increase rapidly. The high temperature object may cause damage to the system and device nearby. Moreover, it may come to a fire, when there is combustible close by the metal object. Therefore, technique to detect the existence of metal object in WPT system is required, which is called as metal object detection (MOD). WPT can not be operated unless the MOD is done and confirming that there is not any metal object.

On the other hand, living object is another challenge to the safety of WPT system. Just as the motivation of the works to restrain the leakage magnetic field in previous chapters, the strong magnetic field will harm the living body. Thus, living object detection (LOD) is required to ensure there is no living object before the WPT starts.

There have been many works proposed to realize foreign object detection (FOD) for WPT system. They can be roughly divided into sensor type and sensor-less type. As for the former,

additional sensor or device are introduced into the system. In [44] and [45], one or multiple groups of coils are placed above the transmitter, and by monitoring the change and pattern of the induced voltages in the detection coils, the existence of metal object can be detected. But these methods, bases on the system parameters like voltages, currents, and inductances, are only effective on MOD usually. Without that obvious influence on the electromagnetic field and the WPT system, LOD is usually realized by using extra sensors like radar [46] and camera [47].

In this thesis, we focus on the researches of MOD, trying to propose techniques that can simply and reliably realize MOD. In the following sections, two works will be introduced. The first is a sensor-less MOD technique adopting on a WPT system without magnetic core, while the second one realizes MOD and misalignment prediction at same time in a WPT system with magnetic core, by using detecting coils. The methods in both works are based on machine learning. The basic idea and the used machine learning methods will be described in the following section as well.

4.1 Object detection to classification problem

The basic idea in our works to realize MOD is treating it as classification problem. Judged as with or without metal object, MOD in WPT system can be considered as a simple binary classification problem. Based on that, machine learning methods can be good choices, if correct and effective parameters are chosen to construct the input vector for classifier.

As proposed in [44] and [45], representing the status of WPT system, the parameters like induced voltages can be good indicator of existence of metal object. A serious challenge to this type of MOD is that, except for the existence of metal object, the misalignment between couplers influences the parameters as well. It requires the MOD method can correctly distinguish the parameters change due to metal object, from that due to misalignment. In this section, a verification work is going to be introduced, where cases with different misalignment and metal

object positions are simulated, and the parameters we expect to indicate the system status are visualized to see if the classification can be realized under the disturbance from coil misalignment.

In the stage of verification of the basic idea – treating MOD as a classification problem – the input impedance of WPT system is chosen to be the characteristic parameter. We considered a WPT system without magnetic core as shown in **Fig. 4.1** (a), and the equivalent circuit of it is same with Fig. 2.3 (b), with capacitor connected to the coils making the system resonant at 85 kHz. For simplification, an aluminum cube as shown in **Fig. 4.1** (b) is used as the foreign metal object, whose eddy current effect is dealt by using complex permeability [48] of sphere approximately, to save the computation time.

(a) Coil (a) The most serious situation

Fig. 4.1 The model of WPT coils

Considering the misalignment ranging from 0 mm to 120 mm, and the metal object placed at 0 mm to 250 mm far away from the center of primary side coil, in total 181 cases with different coil misalignment or position of metal object have been simulated, in which 97 cases are without metal object and the others are with metal object.

All these cases are simulated while the frequency of input current ranging from 85 kHz to 90 kHz with 11 sampling points. In each frequency step for each case, the input resistance and reactance are recorded, and plotted in Fig. 4.2, where corresponding each case, the loci of input impedance are visualized with resistance on the horizontal and reactance on the vertical axis. It

seems that the loci of without metal can be somehow distinguished from the loci of with metal, which means the influence on the input impedance from coil misalignment and from misalignment and metal object together, can be distinguished correctly.

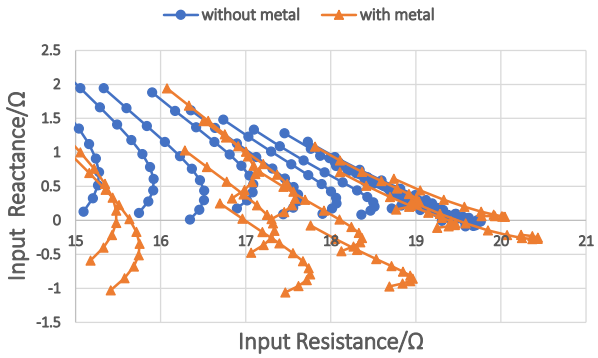

Fig. 4.2 Loci of input impedances

Moreover, using singular value decomposition (SVD), the multi-dimensional vectors of these loci are projected into points in two-dimensional space. By arranging all the vectors together as a matrix K, as described as (4.1). SVD is expressed as (4.2), and the new vectors after dimensional reduction are calculated as (4.3), where only the components of first two orders are used to form the new vectors in two-dimension, shown as points.

$$K = [\boldsymbol{x}_1, \boldsymbol{x}_2, \dots, \boldsymbol{x}_n] \in \mathbb{R}^{22\times n} \tag{4.1}$$

$$K = \mathrm{USV}^t = \sum_{i=1}^{n} \sigma_i \boldsymbol{u}_i \boldsymbol{v}_i^t \tag{4.2}$$

$$\boldsymbol{x}_k \approx \sigma_1 v_{1k} \boldsymbol{u}_1 + \sigma_2 v_{2k} \boldsymbol{u}_2, \ \ 1 \le k \le n \tag{4.3}$$

as shown in Fig. 4.3, it clearly shows that the influence from coil misalignment differs with that from metal object, orienting to different direction on the two-dimensional SVD space. It illustrates the feasibility of the method discussed above. The MOD can be realized by using input impedance, if proper classifier is trained. Whereas, there are several orange points that locate close to the blue

points, which are expected to be the challenge of the classification problem.

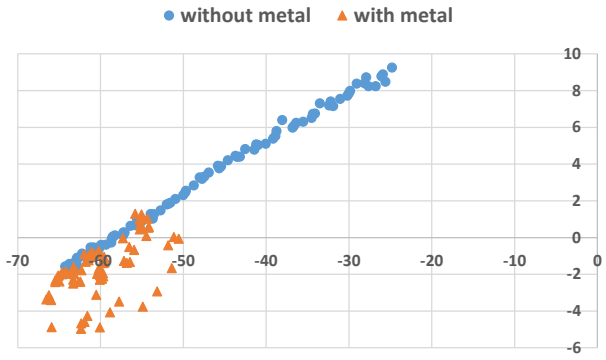

Fig. 4.3 Loci of input impedances

4.2 Machine learning methods

As discussed above, MOD in WPT system can be treated as a supervised classification problem, solved by training classifier using proper methods. This inspired us to adopt machine learning methods, on the training data generated by simulations. Until now, there have been numerous works proposed for developing machine learning methods for classification problem, and application on different specific areas [49].

In this section, the machine learning methods used in the proposed works are going to be introduced. For the programing in this thesis, neural network is constructed using Tensorflow [50], while the other machine learning methods are by Scikit-learn [51].

4.2.1 Support vector machine (SVM)

SVM is a classical method in area of machine learning. When applied to solve classification problem, SVM searches for a (n-1)-dimensional hyperplane which divide the n-dimensional vectors into different classes with the widest gap [52]. In addition, for non-linear classification, a kernel function is usually used to project the input vectors into higher dimensional spaces, where the classification can be turned to linear. In the work in this thesis, radial basis function kernel (RBF kernel) is used for the projection, which is defined as

$$K(\boldsymbol{x}, \boldsymbol{x}') = \exp(-\gamma\|\boldsymbol{x} - \boldsymbol{x}'\|^2) \tag{4.4}$$

where $\boldsymbol{x}$ and $\boldsymbol{x}'$ denote the feature vectors. It is assumed that $\gamma = 1/(n\sigma^2)$, where σ^2 represent the variance of the vectors. After standardization, the variance of the input vector become nearly 1 so that we have $\gamma \approx 1/n$.

4.2.2 Naive Bayes classifier (NBC)

The naive Bayes classifier is based on the Bayes's theorem which state that the posterior probability is given by

$$P(y_i|\boldsymbol{x}) = \frac{P(\boldsymbol{x}|y_i)P(y_i)}{\sum_1^N P(\boldsymbol{x}|y_i)P(y_i)} \tag{4.5}$$

where y_i and $\boldsymbol{x}$ denote the label of classification {0,1}, where 0 (1) corresponds to non-existence (existence) of metallic objects in this thesis, and the feature vector. We assume that likelihood $P(\boldsymbol{x}|y_i)$ obeys the normal distribution, and the prior probability $P(y_i)$ and $P(y_i)$ are determined from the training data. N represents the number of labels of classification. By this way, the likelihood of existing metal object in WPT system can be determined, based on the feature vector, which is constructed by the parameters picked to represent system status.

4.2.3 Gradient boosting decision tree (GBDT)

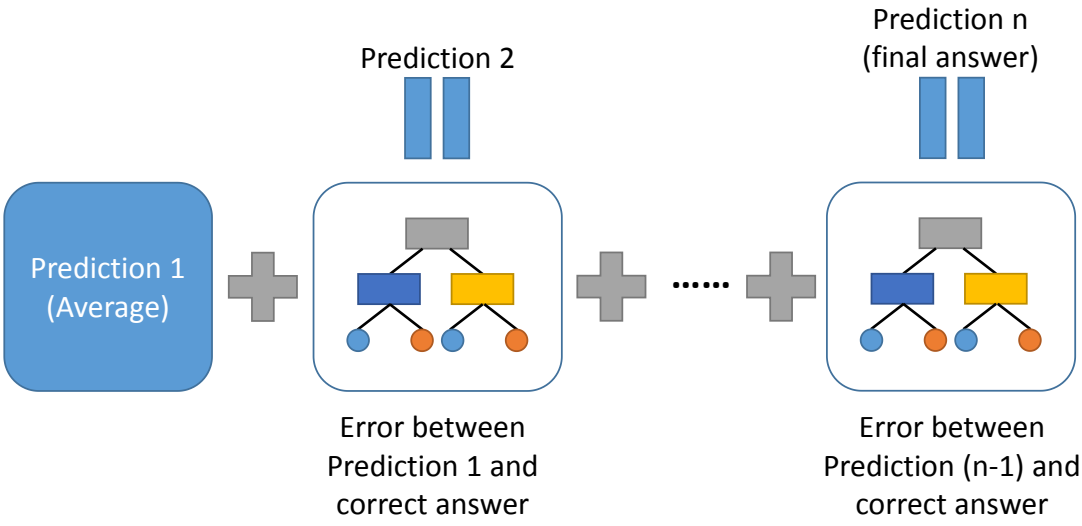

Fig. 4.4 Gradient boosting decision tree © 2022 Japan Society for Simulation Technology

Gradient boosting decision tree (GBDT) is a machine learning method based on gradient

boosting technique and decision tree [53]. Fig. 4.4 schematically shows GBDT. Starting from the first prediction which is set as the average value of all the labels, decision trees are trained in each step to minimize the mean squared error between the correct answer and the prediction obtained in previous step. The sum of all the trees and prediction 1 provides the final answer of GBDT.

In Scikit-learn®, softmax function given by

$$\sigma(\boldsymbol{z})_j = \frac{e^{z_j}}{\sum_{n=1}^{N} e^{z_n}}, \qquad for\ j = 1, \dots, N. \tag{4.6}$$

is used to transform the continuous predicted value to discrete label, when GBDT is applied in classification problem, where N denotes the number of classes, which is 2 in this thesis. The hyper parameters and settings of GBDT are determined by default of Scikit-learn®.

4.2.4 Random forest classifier (RFC)

Random forest (RFC) is an ensemble learning method based on bagging and decision tree [54]. To train each decision tree, the training data is selected randomly with replacement. The split of each tree is found from a random subset of the features, whose size is set as square root of the number of features. By repeating this, we construct many decision trees to compose a random forest. For classification, each tree in the forest gives their own prediction based on the input. The final prediction of the forest is decided by majority vote.

4.2.4 Neural network (NN)

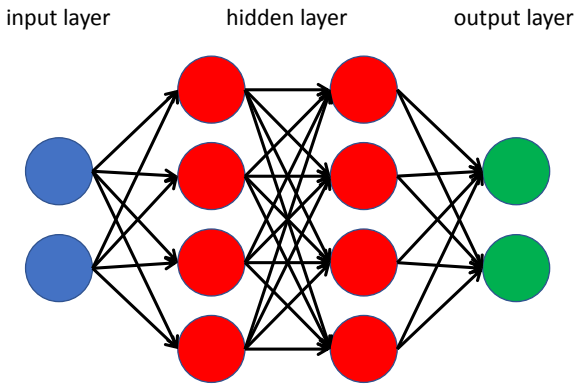

Fig. 4.5 Multilayer perceptron

With the rapid development of machine learning, neural network (NN) is one of the most popular methods, performing well on both regression and classification problem. In our works, besides applied on MOD, NN is used to predict misalignment distance between couplers as well, which will be introduced in next section.

The idea of NN comes from the structure of biological neural circuit. A basic form of NN, as shown in Fig. 4.5, which can be called as multilayer perceptron (MLP), consists of several layers made up by several neurons. Starting from the input layer, vectors are delivered from layers to layers, neurons to neurons, like how the signal is delivered in biological neural circuit. In each neuron, a linear transformation expressed as following equation is done to the input vector $\boldsymbol{v_{in}}$, to get the output vector $\boldsymbol{v_{out}}$.

$$\boldsymbol{v_{out}} = w \cdot \boldsymbol{v_{in}} + b \tag{4.7}$$

where w and b are the parameters of neurons, which need to be adjusted by optimization. Following this, the output vectors are usually transformed one more time, which is called as activation, before they are sent to the neurons in next layer. In our works, Rectified Linear Unit (ReLU) is used as activation function, which is defined as the following.

$$f(x) = \max(0, x) \tag{4.8}$$

By this way, the relationship between the input vectors and output vectors of whole network is constructed. Then, the parameters - w and b - of the neurons in hidden layers will be optimized, according to the loss calculated by training dataset when supervised training. The optimization algorithm used to do this is Adam [55] in our works.

Fitting the output of NN with training data is exactly a regression. When consider classification problems, functions like softmax, as show in (4.6), are used to transformed the continuous output vectors to discrete label.

4.3 Sensorless metal object detection for WPT without magnetic core

In this section, using SVM, NBC, and NN, a sensorless MOD for a WPT system without magnetic core is realized. Sampling at different frequencies around the resonance frequency, the input impedances are recorded, including the real and imaginary part. Collected from FEM simulations, the datasets are used to train and validate the classifiers obtained by the three machine learning methods. Besides, experimental verification is also brought out for in this work.

4.3.1 WPT system and simulation

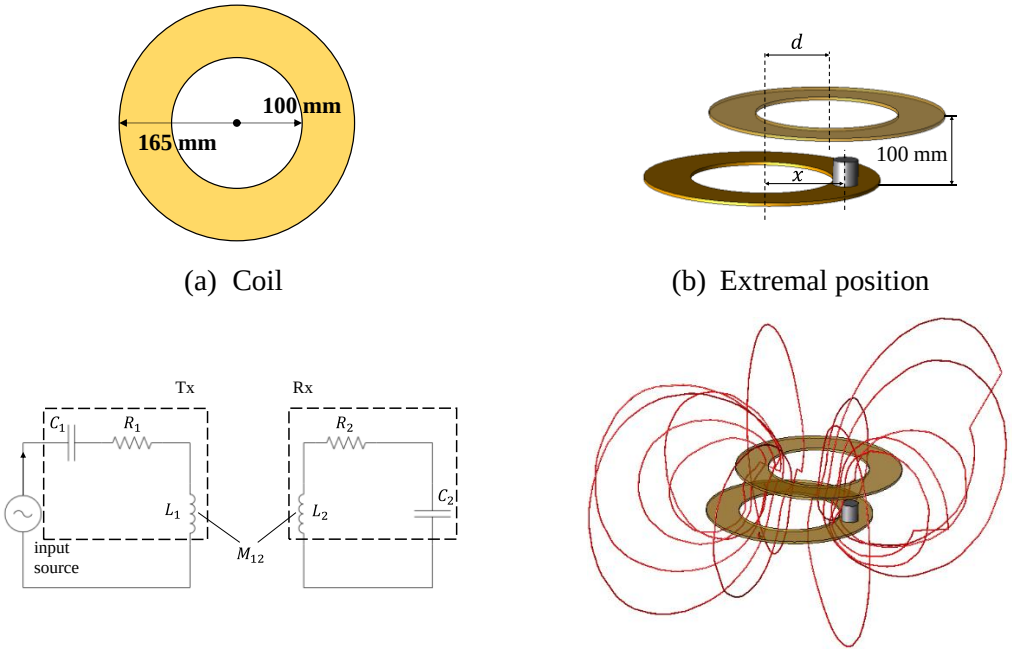

(a) Coil (b) Extremal position

(c) Equivalent circuit (d) Magnetic flux distribution

Fig. 4.6 WPT system model © 2021 Emerald Publishing Limited

A WPT system shown as Fig. 4.6 is considered, where an aluminum cylinder with a diameter and height of 35 mm is used as the foreign metal object. The parameters of the WPT system and the circuit are summarized in Table 4.1. The capacitance is adjusted to make the system resonate at 81 kHz, which is same with the experimental system.

Table 4.1 Parameters of WPT © 2021 Emerald Publishing Limited

Inner radius of coil	100 mm
Outer radius of coil	165 mm
Turns of coil	16
Transmission distance	100 mm
Input source (current)	I_{rms}=20 mA
R_1, R_2	1 Ω
C_1, C_2	45 nF

Like the verification of basic idea described in section 4.1, in this work, 116 cases have been simulated using JMAG®, with sampling frequencies ranging from 75 kHz to 85 kHz. Vectors to represent the cases are constructed as

$$\boldsymbol{Z} = [R_1, \dots, R_{11}, X_1, \dots, X_{11}]^t \in \mathbb{R}^{22} \tag{4.6}$$

where R_i and X_i are the input resistance and reactance of WPT system, while i is the index of sampling frequency point. Finally, like what is shown in section 4.1, Fig. 4.2, the impedance loci of the simulation cases are shown in the figure below. It shows that the cases with and without metal object seem to be distinguishable, though the effect of coil misalignment exists as well.

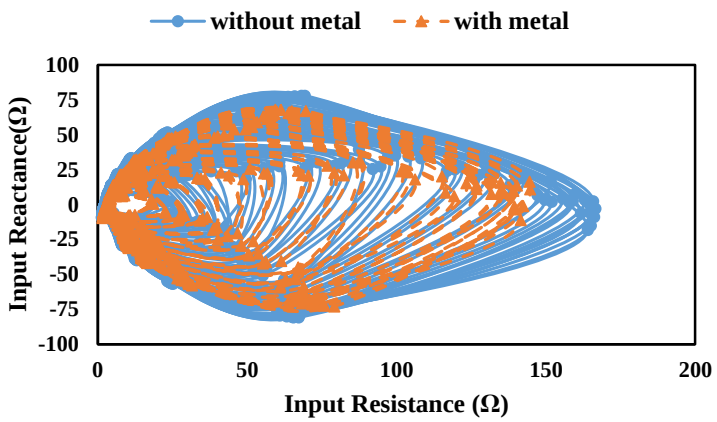

Fig. 4.7 Impedance loci (simulation) © 2021 Emerald Publishing Limited

4.3.2 machine learning classifiers

In this work, SVM, NBC and NN are used to train the classifier. The structure of used NN is shown as Fig. 4.8, where three dense layers are placed with activation function as ReLU. The simulation data are divided into training dataset and validation dataset according to a proportion of 80%:20%. And the exact value of γ in the equation 4.1, which is the definition of RBF kernel used in SVM, are listed in Table 4.2.

Table 4.2 value of $\gamma^2 = 1/\sigma^2$

Simulation, no load	0.0442
Simulation, 20Ω load	0.0439
Experiment, cylinder	0.0449
Experiment, can	0.0490
Experiment, key	0.0477
Simulation, no load	0.0442

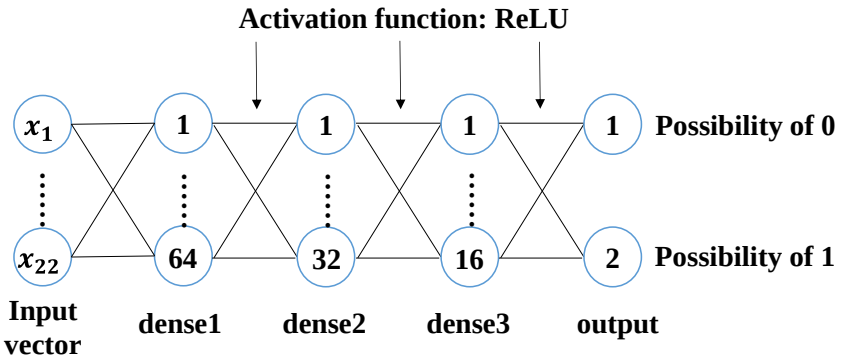

Fig. 4.8 Structure of NN

4.3.3 Classification results (simulation)

As described above, the simulation data have been used to train classifiers using the three machine learning methods. The accuracy of trained classifiers for the validation dataset are

compared and shown in Table 4.3, where NN obtained the best performance of 100%, while SVM and NBC obtained 96% and 88% respectively.

Table 4.3 Accuracy of three methods for validation data (simulations)

NN	100%
SVM	96%
NBC	88%

4.3.4 Classification results (experiment)

An experimental verification of the proposed method is described in this section. The WPT coils and associated circuit are same with the simulations. The coils, LCR meter, and the metal object used in the experiments are shown in Fig. 4.9, with the specific size of metal objects marked.

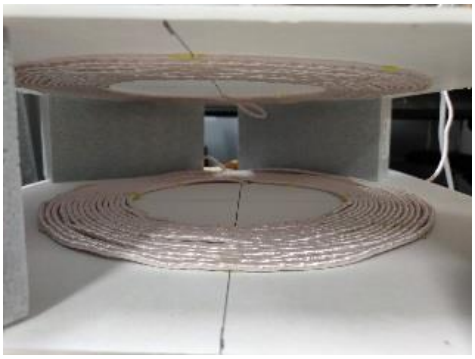

(a) WPT coils

(b) LCR meter (HIOKI IM3536)

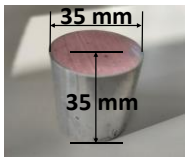

(c) Cylinder

(d) Can

(e) Key

Fig. 4.9 Experiment devices

A) Aluminum cylinder

Firstly, totally same with what is considered in the simulations, an aluminum cylinder is tested. The aluminum cylinder is placed 0 mm, 130 mm and 200 mm away from the center of primary coil, which is set to the same as the simulations. The input impedance values for 131 cases have been measured here, where 33 cases are without metal and 98 cases are with metal.

The input impedance loci of the 131 cases are shown in Fig.11. The tendencies in the loci obtained from the simulation and experiments seem similar although there are quantitative differences between them which are possibly caused by factors such as skin effect and noise of devices. The differences in the loci for the cases with and without metal object are unclear though NN still obtains good performance as described below.

The performances of three methods are listed in Table 4.4. NN still got the best accuracy this time, but obvious decrease on the accuracy of SVM and NBC can be seen, which demonstrates that NN has a larger potential for classification problem. And the accuracy of NN seems hard to maintain 100% accuracy when partition of dataset changes. However, the minimum accuracy of 96% by NN still prove the effectiveness of our method.

Table 4.4 Accuracy of three methods for validation data (experiment, cylinder)

NN	96% ~ 100%
SVM	70%
NBC	58%

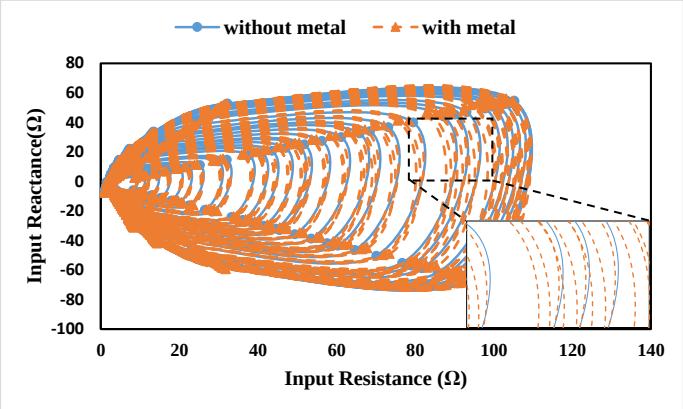

Fig. 4.10 Impedance loci (experiment, cylinder) © 2021 Emerald Publishing Limited

B) Empty aluminum can

When using the empty aluminum can as the foreign metal object, the input impedance loci show obvious differences between cases without and with metal as shown in, where 101 cases are measured, including 33 and 68 cases without and with metal. The can is laid in experiments, and placed in the center of Tx coil, or 100 mm far away from the central axis.

It seems easier for NN to make correct judgement for the cases. In Table 4.5, it can be seen that all the three machine learning methods have accuracy over 90%. These results come from the clear difference in the loci shown in Fig. 4.11. However, it would be difficult for us to pick the features from the loci for classification. The machine learning methods automatically take those features from the data.

Table 4.5 Accuracy of three methods for validation data (experiment, can)

© 2021 Emerald Publishing Limited

NN	100%
SVM	100%
NBC	90%

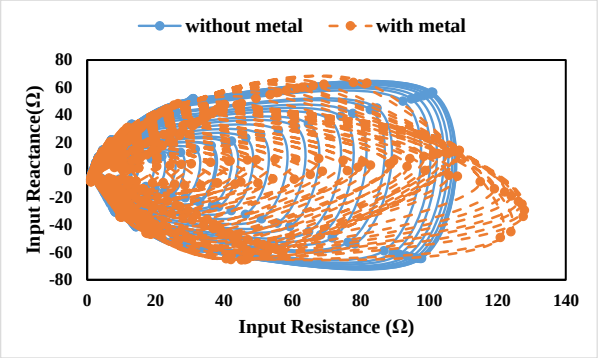

Fig. 4.11 Impedance loci (experiment, can) © 2021 Emerald Publishing Limited

C) Steel key

In the experiments with key, the positions of the key are set to the same as the cylinder cases. In total, 136 cases are measured, including 34 without metal and 102 with metal.

The input impedance loci of all the cases are shown in Fig. 4.12. It seems hard to find the differences between the loci without and with metal. As a result, as shown in Table 4.6, all the three machine learning methods judge all the cases in validation as with metal, so the accuracy of them are all 71%, which is exactly the proportion of cases with metal in the validation dataset.

Table 4.6 Accuracy of three methods for validation data (experiment, key)

© 2021 Emerald Publishing Limited

NN	71%
SVM	71%
NBC	71%

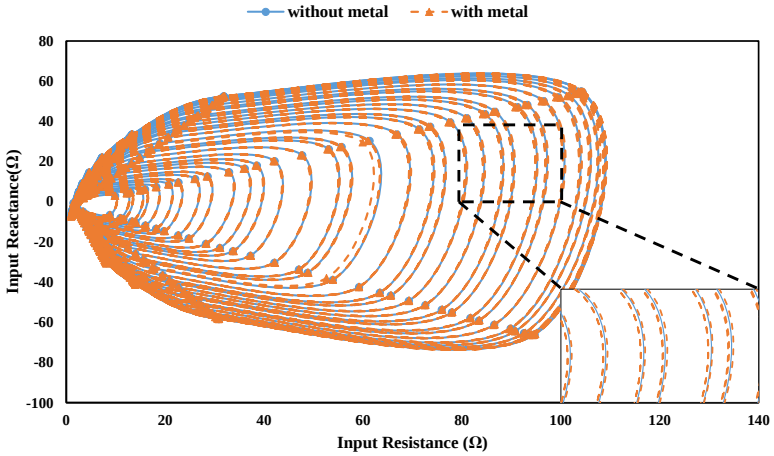

Fig. 4.12 Impedance loci (experiment, key) © 2021 Emerald Publishing Limited

4.3.5 Conclusion

In this section, a work of MOD technique for WPT system without magnetic core is introduced. Using SVM, NBC, and NN to train the classifiers, both simulation and experiment verifications have been done, and the results show that NN always has the highest accuracy above 90% among the three methods. Nonetheless, when a steel key is used as the foreign metal object, all the three machine learning methods failed to obtain effective classifier. Improved method requires to be considered to solve this problem.

4.4 Metal object detection for WPT with magnetic core

In this section, MOD considering WPT systems with magnetic core will be introduced. After the proposed work discussed in previous section, we found that the sensor-less method seems hard to obtain similar performance when applied to WPT system with magnetic core. A possible reason for that is that the existence of ferrite makes the distribution of magnetic field not homogeneous for all directions, so the influence from misalignment and metal object become difficult to be distinguished, only depending on the input impedance.

For this reason, a simple detection coils group is introduced into the WPT system. Using

differential voltage of the detection coils group as a new signal, MOD is successfully realized. And the accuracies of MOD using input impedance or differential voltage, or both, are compared to see the contribution of two types of signals.

4.4.1 WPT system model

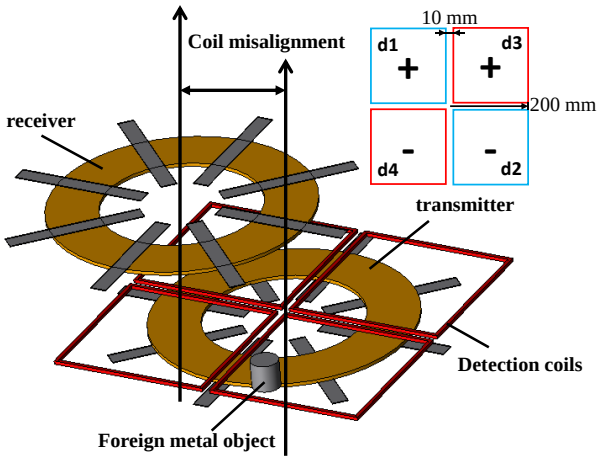

(a) WPT system and detection coils

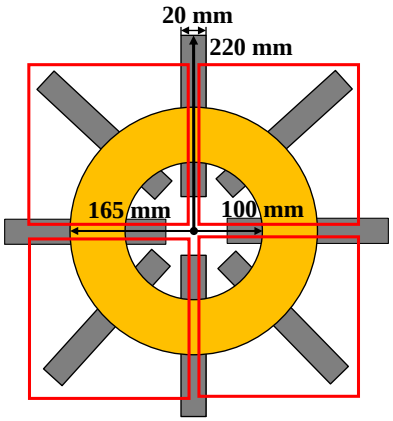

(b) WPT coupler

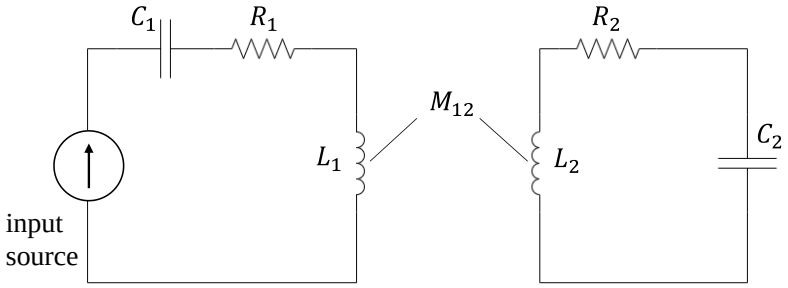

(c) Circuit model

Fig. 4.13 WPT model © 2022 Japan Society for Simulation Technology

As mentioned above, a WPT system which is different with that in previous works is considered. As shown in Fig. 4.13, several bar-shaped ferrites with relative permeability of 3300 are placed near the transfer coils, which is a common design to improve the transfer efficiency of WPT

system. The gap between two coils is 100 mm, and the metal object is considered as an aluminum cylinder with diameter and height of 35 mm.

Above the primary coupler, a group of detection coils are settled. The directions of the detection coils are denoted in Fig. 4.13 (a), consisting of four one-turn coils which are divided into two pairs marked by different colors. This design has been used in many works of MOD like [44] and [56]. In each pair, the two coils have opposite winding directions, and are connected in series to get differential voltage, which is the sum of induced voltage in two coils. When there is no coil misalignment and any metal object, the magnetic flux passing through each coil are equal, making the induced voltages have equal values but opposite phases, so the differential voltages of pairs become zero as a result. Nevertheless, when there is coil misalignment or metal object, the differential voltage would not be zero anymore because of the unequal magnetic flux through the coils. Therefore, the differential coils can be used in WPT system to provide differential voltages as a signal to represent the status of magnetic field inside the system.

About the circuit setting, as shown in Fig. 4.13 (c), it is a resonance system with capacitances connected to coils to make the system resonating at 85 kHz. In this work, the effect of the existence of load resistance is going to be discussed. The simulations will be run with and without a load resistance of 20 Ω connected, respectively.

4.4.2 Simulations

In the simulations, the coil-misalignment ranges from 0 to 80 mm in any direction, while the metal object is randomly placed within the space covered by the detection coils. In total, 901 cases with different coil misalignments and different positions of metal object, and 677 cases without metal object are simulated, for no-load condition where the receiver coil is shorted. And for load condition, 677 cases without metal and 625 cases with metal are simulated. All the simulations use JMAG® as the solver of field computation.

The differential induced voltage V_{d12} at 75, 85 and 100 kHz in the pair d1- d2 for the no-load condition are plotted in (a) of Fig. 4.14, Fig. 4.15 and Fig. 4.16 where the horizontal and vertical axes represent the real and imaginary part of V_{d12}, respectively. The differential voltages V_{d34} for the pair d3-d4 is found to have the similar tendency as that for V_{d12}, as shown in (b) of Fig. 4.14, Fig. 4.15 and Fig. 4.16.

Without obvious difference like when input impedance is plotted, it seems hard for people to distinguish the cases with and without metal according to differential voltages. For this reason, machine learning methods are expected to realize the classification.

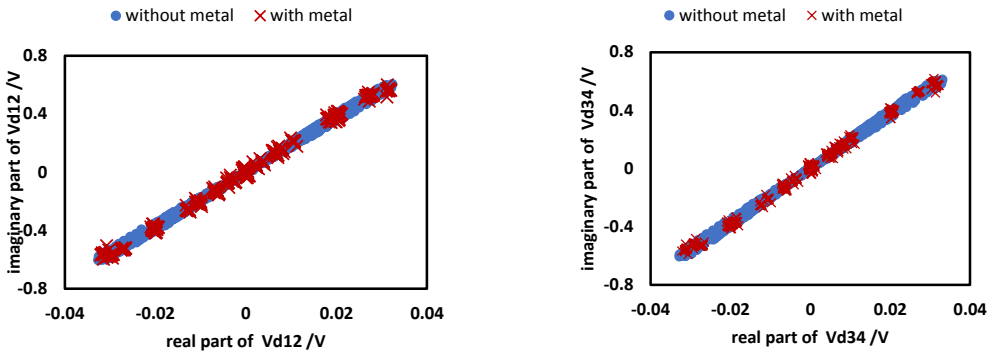

(a) pair d1-d2 (b) pair d3-d4

Fig. 4.14 Differential induced voltages at 75 kHz for different cases

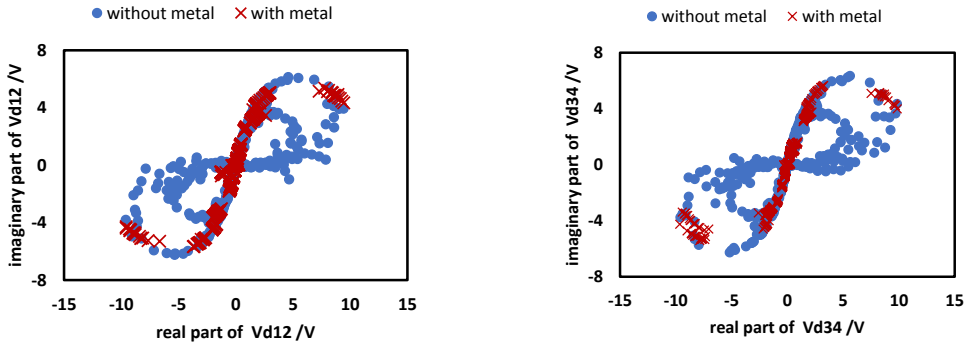

(a) pair d1-d2 (b) pair d3-d4

Fig. 4.15 Differential induced voltages at 85 kHz for different cases

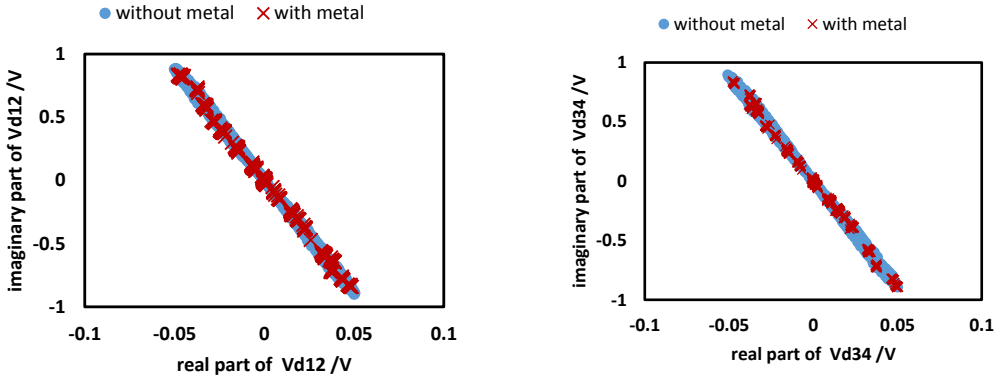

(a) pair d1-d2 (b) pair d3-d4

Fig. 4.16 Differential induced voltages at 100 kHz for different cases

4.4.3 data preparation and machine learning

The process of proposed method is shown in Fig. 4.17. Three types of feature vectors will be considered in the verifications, which are only input voltage of system, only differential voltage, and both. By sampling the frequency range of 75 to 100 kHz in 11points with equal increments, three 22-dimensional vectors are constructed as followings:

$$\boldsymbol{V_1} = [u(1,1), \dots, u(1,11), v(1,1), \dots, v(1,11)\,] \tag{4.7}$$

$$\boldsymbol{V_2} = [u(2,1), \dots, u(2,11), v(2,1), \dots, v(2,11)\,] \tag{4.8}$$

$$\boldsymbol{V_3} = [u_{in}(1), \dots, u_{in}(11), v_{in}(1), \dots, v_{in}(11)] \tag{4.9}$$

where $\boldsymbol{V_1}$ and $\boldsymbol{V_2}$ consist of the real $u(i,j)$ and imaginary part $v(i,j)$ of the differential voltage of pair i at sampling frequencies identified by $j = 1,2,\dots,11$. Moreover, $\boldsymbol{V_3}$ is composed of the real and imaginary part of the input voltage of the primary coil.

These feature vectors will be standardized to make the input vectors for classifier training. In this work, four machine learning methods (SVM, NBC, GBDT, RFC) are used for the training. The parameters used in the training by GBDT and RFC are listed in Table 4.6 and Table 4.8. All these methods are implemented by scikit-learn® [51] in Python.

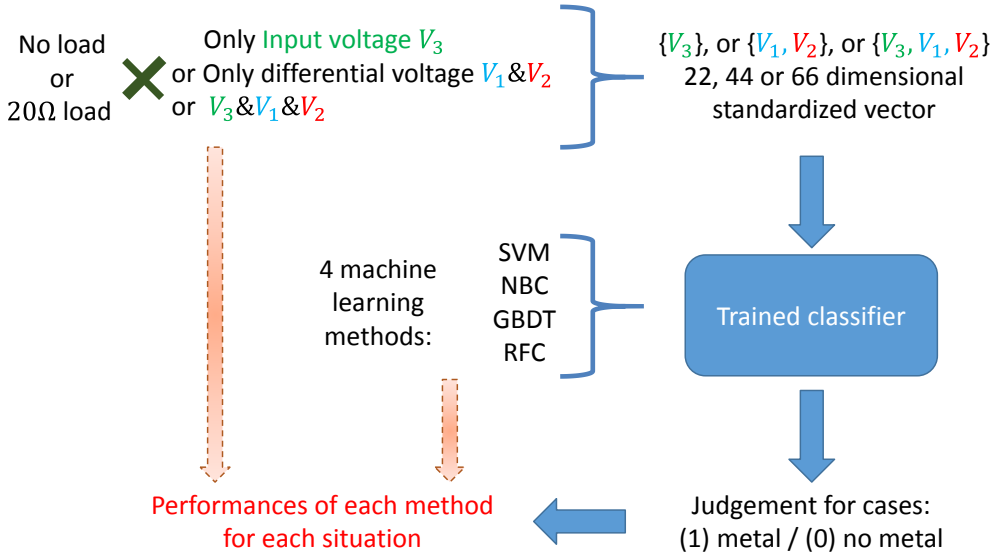

Fig. 4.17 Process of proposed method

Table 4.7 Hyper parameters and setting of GBDT

Loss function	Logistic regression	Number of boosting stages	100
Learning rate	0.1	Maximum depth of estimators	3
Function to evaluate split	mean squared error with improved by Friedman [57]	Minimum Number of samples to split a node	2

Table 4.8 Hyper parameters and setting of RFC

Number of trees	100	Number of features for finding split	Square root of the dimension of input
Maximum depth of the tree	None	Minimum Number of samples to split a node	2
Function to evaluate split	Gini impurity	minimum number of samples required to be at a leaf node	1

4.4.4 Training and validation

4.4.4.1 K-fold cross validation

To eliminate the influence of division between training and validation data on the performance of classifiers, K-fold cross validation is used in this work. All the data are divided into 10 subsets while the proportion of each class in the subsets remain same as that in the entire dataset. Classifiers obtained by each machine learning methods will be trained for 10 times, while each subset will be used as validation data in order and the others as training data at the same time. Finally, the average accuracy of the 10 times training is treated as the final accuracy of the methods.

4.4.4.2 Classification results

As mentioned before, different input vectors and their combination are used for the training

respectively, to see the effect under no-load and 20 Ω load conditions. Finally, applying K-fold cross validation, the results are summarized in Table 4.9. Overall, only GBDT and RFC can obtain good accuracy, while SVM and NBC failed to get accuracy over 80%. And it shows that when all the feature vectors constructed by input voltages and differential voltages are inputted, the trained classifiers obtained highest accuracies, compared to other input patterns. And an obvious difficulty of training can be seen when only the input voltages are inputted and load resistance are attached, which demonstrate that only inputting $\boldsymbol{V_3}$ is incompatible with our proposed method. The reason for this is since there are little differences in $\boldsymbol{V_3}$ because of the off-resonant states. By introducing the differential voltages into the input data, we can perform accurate classification.

However, highest accuracy is obtained when $\{\boldsymbol{V_1}, \boldsymbol{V_2}, \boldsymbol{V_3}\}$ is inputted to training by GBDT and RFC, where GBDT reached 93.8% and 97.9% by RFC. The reason why the two decision-tree based methods performed better is considered to be that weak classifier is more suitable for this problem.

Table 4.9 Accuracy of trained classifiers

Load conditions	20Ω load	No load (shorted)
Case I: $\{\boldsymbol{V_3}\}$ (22 dimensions)	SVM=60.5%	SVM=77.9%
	NBC=60.5%	NBC=56.5%
	GBDT=82.5%	GBDT=93.5%
	RFC=84.0%	RFC=94.2%
Case II: $\{\boldsymbol{V_1}, \boldsymbol{V_2}\}$ (44 dimensions)	SVM=51.2%	SVM=57.1%
	NBC=50.8%	NBC=48.4%
	GBDT=93.4%	GBDT=89.2%
	RFC=97.2%	RCF=95.0%
Case III: $\{\boldsymbol{V_1}, \boldsymbol{V_2}, \boldsymbol{V_3}\}$ (66 dimensions)	SVM=63.4%	SVM=68.2%
	NBC=56.3%	NBC=54.8%
	GBDT=93.8%	GBDT=94.1%
	RFC=97.9%	RFC=95.8%

Then, using SVD, which is introduced in section 4.1, a validation dataset is projected into two-dimensional space, as shown in Fig. 4.18, and the predictions of each classifier trained by each machine learning method are marked according to if it is correct or not. It shows that SVM and NBC tend to classify the data by a high dimensional plane, which is somehow projected into the two-dimensional space as a straight line, after SVD. However, the classification by GBDT and RFC don't show such division based on straight line, which may be the reason why they have higher accuracy.

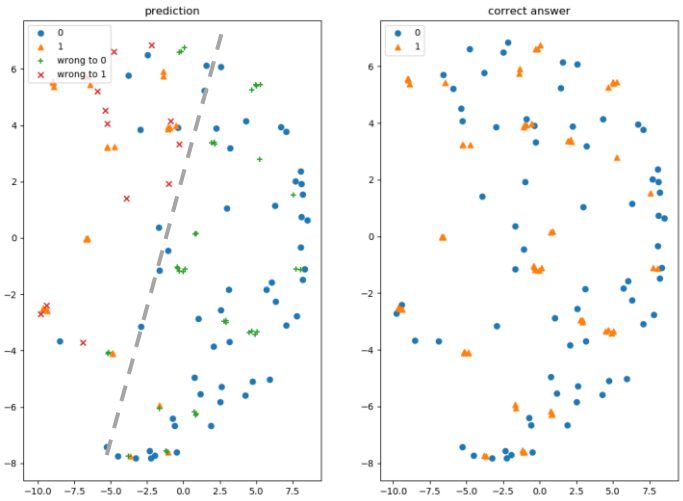

(a) SVM

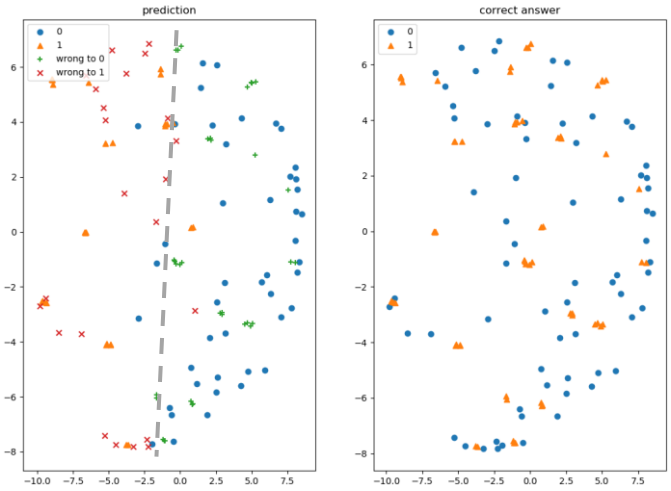
prediction
correct answer
0
1
wrong to 0
wrong to 1

(b) NBC

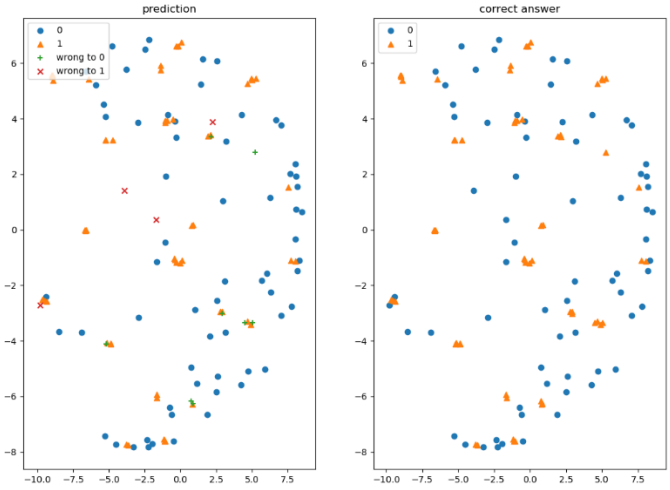
prediction
correct answer
0
1
wrong to 0
wrong to 1

(c) GBDT

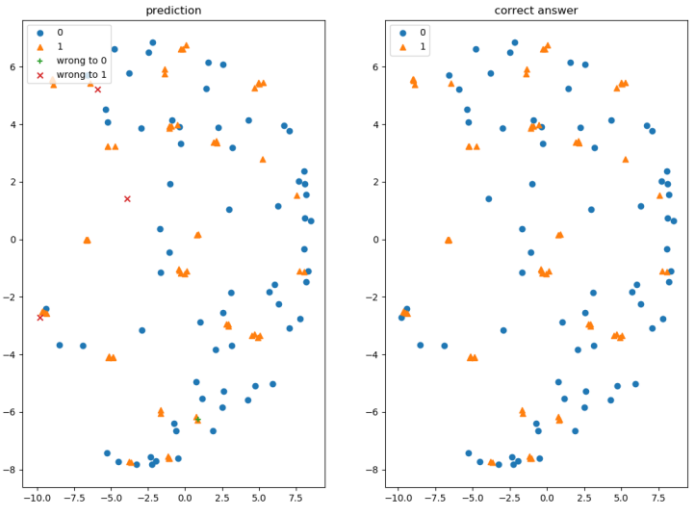

(d) RFC

Fig. 4.18 Visualizations of classification by SVD

4.4.5 Conclusion

In this section, we introduced a work of MOD considering WPT system with magnetic cores. Unlike the works in previous sections, in order to overcome the difficulties brought by introducing magnetic cores in system, detection coils are applied, providing new feature signal of system other than input status of system (impedance or voltage). Four machine learning methods have been used to train the classifiers. Finally, GBDT and RFC obtain good accuracies compared to SVM and NBC. And the introduction of differential voltages from detection coils was proved to be effective for improving MOD accuracy.

4.5 MOD and misalignment prediction together

As discussed before, coil misalignment may bring obvious influence on the performances of WPT system including the transfer efficiency and the safety. Thus, techniques to detect, predict the exact misalignment distance can help to adjust the WPT system to better and safer status. Some works have been proposed to realize simple misalignment distance prediction. In [58], the misalignment was predicted from the voltage induced in the sensor coils near the winding on the

primary coil, where the extreme gradient boost algorithm was employed for the prediction. Similar sensor coils were used for MOD [59]. Like these two works, the detection coils introduced into WPT system for MOD, can be adopted to the misalignment distance prediction at same time, using same feature signals same as for MOD.

In this section, following the work described in previous section, a similar WPT system with similar detection coils are considered. And neural network is used to realize MOD and misalignment distance prediction simultaneously, by treating the former as classification problem, and the latter as regression problem.

4.5.1 WPT system model

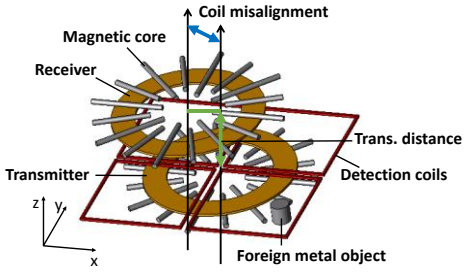

Fig. 4.19 WPT system model © 2022 IEEE

(a) 15 turns (L ≈ 86.9 μH) (b) 10 turns (L ≈ 52.1 μH)

Fig. 4.20 WPT coupler © 2022 IEEE

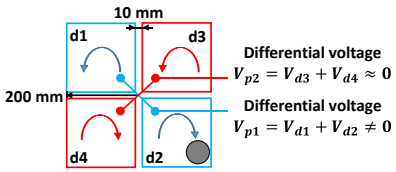

Fig. 4.21 Differential coils © 2022 IEEE

A model shown in Fig. 4.19 - Fig. 4.21 is consider in this work. The system is adjusted to resonate at 85 kHz, and a 20 Ω resistor is connected to receiving coil as the load. Instead of flat ferrite, pole-shaped ferrite is used here, while the relative permeability of them is set as 3300. 15 turns coil and 10 turns coil are modeled respectively, as shown in Fig. 4.20, where r_{in} and r_{out} which denote the inner and outer radius of coils are 77.5 and 145 mm for 15 turns, while they are 100 and 145 mm for 10 turns. The effectiveness of proposed method on them will be discussed after.

A similar design of detection coils is used, as illustrated in Fig. 4.21. Four one-turn coils are placed, with the diagonal ones of them are paired as $p_1(d1, d2)$ and $p_2(d3, d4)$. Differential induced voltages of these two pairs are computed in each simulation case, and used as feature signals to realize MOD and misalignment distance prediction.

An aluminum cylinder with a diameter of 35 mm and height of 35 mm is assumed as the foreign metal object. This object has similar or smaller size in comparison with a can and bar listed in IEC 61980-3 [18]. The eddy current in the aluminum cylinder is considered in the field computation using JMAG®.

4.5.2 Data preparation

The transfer distance ranges from 50 to 100 mm, namely the distance assumed to be 75 ±25 mm，while the coil misalignment on the x-y plane ranges from -70 to 70 mm. The metal object is assumed to have a random position within the space covered by the detection coils.

Totally, 1500 cases have been simulated, half with and half without a foreign metal object. An

operating frequency of 85 kHz is considered in all the cases, where differential voltages of detection coils pairs and the input voltage of system are recorded to construct the feature vectors as the followings.

$$\boldsymbol{V}_{in} = \left[u_1^r, u_1^i, u_2^r, u_2^i, \ldots\right] \tag{4.10}$$

$$\boldsymbol{V}_p = \left[v_{11}^r, v_{11}^i, v_{12}^r, v_{12}^i, v_{21}^r, v_{21}^i, v_{22}^r, v_{22}^i, \ldots\right] \tag{4.11}$$

where the quantities with indexes r and i denote the real and imaginary components, $\boldsymbol{V}_{in}$ is composed of the input voltages $u_k = u_k^r + ju_k^i$ of the primary coil, while $\boldsymbol{V}_p$ consists of the differential voltages $v_{kl} = v_{kl}^r + jv_{kl}^i$ of the l-th pair for the cases $k = 1,2, \ldots$.

Like what we did in previous sections, the vectors $\boldsymbol{V}_p$ for the 15 turns coils are mapped on the two-dimensional plane by singular value decomposition (SVD) as shown in Fig. 4.22. Fig. 4.22 (a) shows the distribution of cases with and without metal object, where each point corresponds to each case, and the distinguishment between them can be seen somehow. In Fig. 4.22 (b) and (c), the points are colored by the misalignment distance in the cases, while (b) shows the misalignment distance in x direction, which should have similar pattern with that in y direction, and (c) shows the ground clearance variation. These two figures illustrate clear correlation between the feature vectors and the misalignment and variation, but not for the existence of metal object, at least in the two-dimensional plane obtained by SVD.

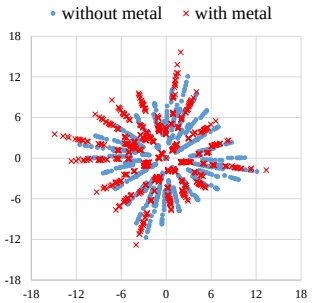

(a) Marked according to the existence of a metal object

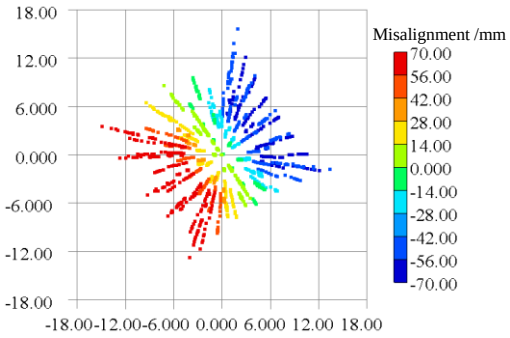

(b) Marked according to misalignment in the x direction

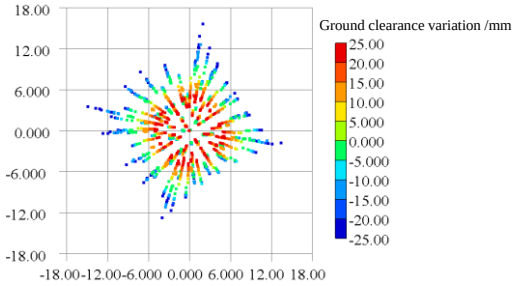

(c) Marked according to variance on clearance in the z direction

Fig. 4.22 Visualization of $\{V_p\}$ through SVD © 2022 IEEE

4.5.2 Neural network

We implemented an NN using Tensorflow® [50] and Python. The hyperparameters are listed in Table 4.10, and the structure of the NN is shown in Fig. 4.23. The input data are either $\{\boldsymbol{V}_{in}, \boldsymbol{V}_p\}$ or $\{\boldsymbol{V}_p\}$, which are standardized before being provided to the NN, and $\boldsymbol{D}_{in}$ denotes the dimensions of input vectors. We configured four dense layers composed of 64 neurons whose activation function was set to ReLU. The NN has four outputs representing the existence possibility of the metal object, the misalignment distances, and the clearance variance in z direction. The loss functions and weighting coefficients for the losses are included in Table 4.10 as well.

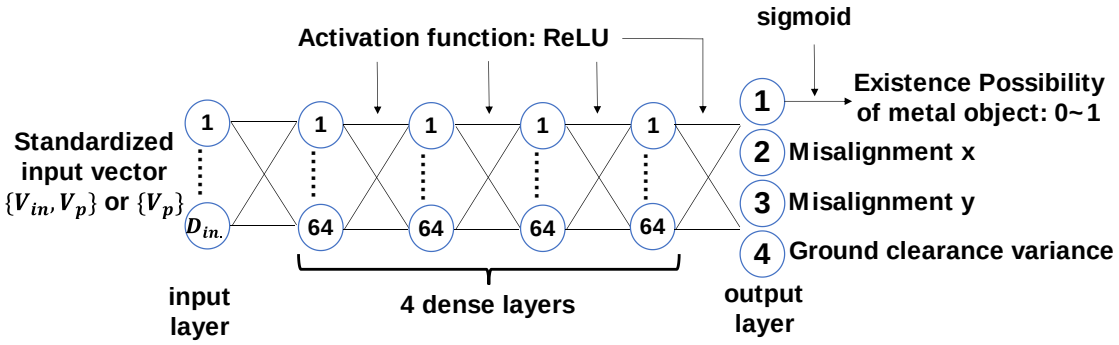

Fig. 4.23 NN structure

Table 4.10 Hyperparameter of the NN © 2022 IEEE

Batch size	20
Epochs	750
Optimizer	Adam
Learning rate	0.001
Loss function (MOD)	Binary cross entropy
Loss function (position prediction)	Huber loss
Loss weights (MOD : position prediction)	1 : 0.01

4.5.3 Training and validation

4.5.3.1 K-fold cross validation

Same with the work introduced in previous section, K-fold cross validation is used here to eliminate the influence of division of training and validation dataset. For both 15-trun and 10-turn coil models, 5-fold cross validation was applied to the trained NNs. The average performances in the 5 times validation are treated as the final performance of the NNs in this section. The program was implemented by using Scikit-learn® [51].

4.5.3.2 Training results

The performance of the trained NNs is shown in Table 4.11, which includes the accuracy of MOD and the mean absolute error in the prediction of misalignment distances (Error in x, y) and clearance variance (Error in z). For both result types, the accuracy of the 15-turn model is better than that of the 10-turn model. The accuracy of MOD for the former model is over 90% for both

cases based on $\{\boldsymbol{V}_{in}, \boldsymbol{V}_p\}$ and $\boldsymbol{V}_p$ while that for the latter is between 80% and 85%. This is because the 15-turn model has a larger inductance, so that a larger magnetic field is generated between the coils, causing a larger eddy current loss in the metal object. This results in a larger change in $\boldsymbol{V}_{in}$ and $\boldsymbol{V}_p$ caused by the metal object. For this reason, MOD becomes easier.

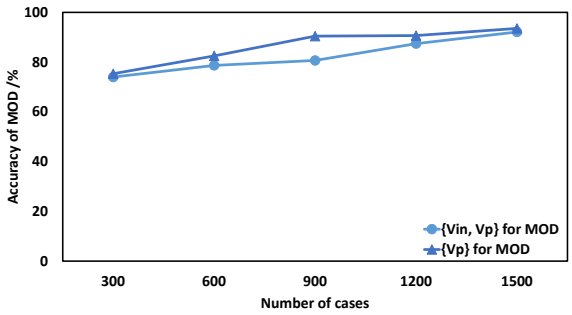

(a) Accuracy of MOD

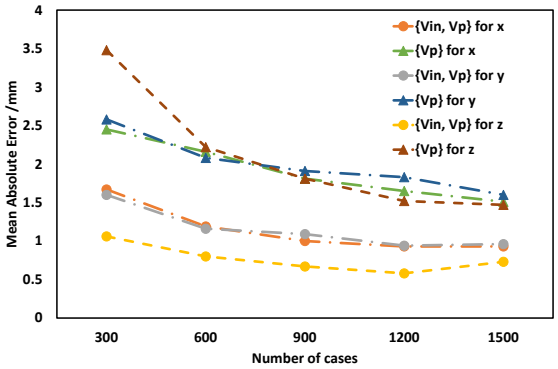

(b) prediction error in the *x*, *y* misalignment, and clearance variation in *z*.

Fig. 4.24 Dependence of performance on number of cases for the 15-turn model

Table 4.11 MOD accuracy and error in position prediction of trained NN © 2022 IEEE

	15-turn coil	10-turn coil
Case I: $\boldsymbol{V}_p$ (4 dimensions)	MOD: 93.54%	MOD: 80.9%
	Error in x: 1.51 mm	Error in x: 6.75 mm
	Error in y: 1.60 mm	Error in y: 7.14 mm
	Error in z: 1.47 mm	Error in z: 3.45 mm
Case II: $\{\boldsymbol{V}_{in}, \boldsymbol{V}_p\}$ (6 dimensions)	MOD: 92.13%	MOD: 84.39%
	Error in x: 0.93 mm	Error in x: 1.00 mm
	Error in y: 0.96 mm	Error in y: 1.07 mm
	Error in z: 0.73 mm	Error in z: 0.69 mm

The prediction accuracy for the misalignment distance and clearance variance was clearly improved by adding $\boldsymbol{V}_{in}$ to the input data. This tendency is more remarkable in the 10-turn model; the prediction error is reduced to less than 20% by using $\boldsymbol{V}_{in}$ in addition to $\boldsymbol{V}_p$. These results suggest that the use of $\{\boldsymbol{V}_{in}, \boldsymbol{V}_p\}$ as the input data is preferable for our purpose. It is noted that the predicted misalignment and clearance variance error in z direction can be sent to the user of the WPT, who can make a fine alignment to improve the energy transfer efficiency.

Next, we consider the dependence of performance on the amount of data. We randomly thin the data to create new data sets with sizes ranging from 300 to 1500 cases. NNs were trained and evaluated using the different numbers of cases. Fig. 4.25 shows the dependence of the performance of the trained NN for the 15-turn model on the number of cases. The accuracy of the MOD increases, and the prediction error in the alignment distance decreases, with the number of cases. A similar tendency was observed for the 10-turn model.

4.5.3.3 Misalignment and clearance variance prediction

In some scenarios like factory, there is unlikely to be foreign metal object in WPT system. And

it is more important to get precise misalignment and clearance variance prediction, for ensuring the transfer efficiency. For this reason, without MOD, the performance of the proposed method on misalignment and clearance variance prediction is evaluated, using the simulation data without metal object. The structure and parameters of NN remain unchanged, except for setting the loss weight of MOD to 0, to build a NN specialized in the position prediction only.

The results are summarized in Table 4.12. Compared to the NN mentioned in the previous section, it has higher accuracy in the prediction of misalignment distances and clearance variance, especially when the combined data $\{\boldsymbol{V}_{in}, \boldsymbol{V}_p\}$ are used for the input data to the NN.

Fig. 4.25 shows the dependence of the error in the position prediction on the number of cases when using $\{\boldsymbol{V}_{in}, \boldsymbol{V}_p\}$. The accuracy depends on the number of turns. For the 15-turn model, the error can be reduced to 0.5 mm by increasing the number of training data cases.

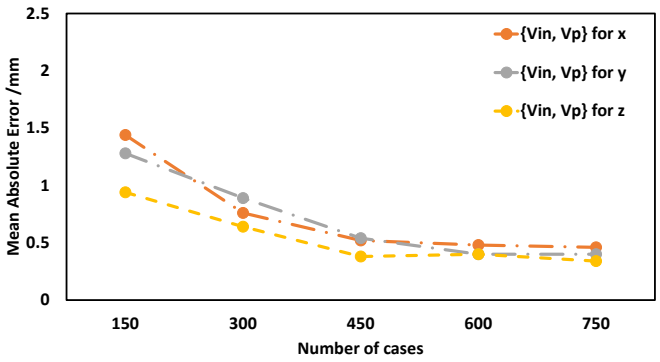

Fig. 4.25 Dependence of misalignment distance error in the *x*, *y*, and clearance variation in *z* on the number of cases (15turns, without MOD) © 2022 IEEE

Table 4.12 Accuracy and error in position prediction of trained NN (without MOD)

	15-turn coil	10-turn coil
Case I: $\boldsymbol{V}_p$ (4 dimensions)	Error in x: 1.51 mm	Error in x: 6.75 mm
	Error in y: 1.60 mm	Error in y: 7.14 mm
	Error in z: 1.47 mm	Error in z: 3.45 mm
Case II: $\{\boldsymbol{V}_{in}, \boldsymbol{V}_p\}$ (6 dimensions)	Error in x: 0.93 mm	Error in x: 1.00 mm
	Error in y: 0.96 mm	Error in y: 1.07 mm
	Error in z: 0.73 mm	Error in z: 0.69 mm

4.5.3.3 Effect of noise

In the real scenario, there may be lots of noise happened during the measurement. To know the effect of those noise in the data on the training results, and how robust the proposed method is, random noise is added to the original data. The noise level was mapped to the equivalent size variation in the foreign metal object, both of which cause the same change in the input and differential voltages. We considered the two different noise levels which are equivalent to the size variation ranging from 32 to 35 mm for the input voltage and 30 to 35 mm for the differential voltage in Case A, and the size ranging from 25 to 35 mm for the input voltage and 20 to 35 mm for the differential voltage in Case B. It is assumed that there is no misalignment and the metal object is placed at a certain position. The results are summarized in Table VI. It can be seen that there is no significant differences in the accuracy of MOD, while that of the misalignment prediction clearly becomes worse with the noise level. However, the latter error is still lower than 4 mm. The prediction accuracy depends on the noise level in the real environment, which should be measured for the design of this detection system.

Table 4.13 Accuracy for MOD and position prediction under noisy environment (15 turns)

	Original data	Case A	Case B
MOD	92.13%	88.9%	94.1 %
Error in x	0.93 mm	2.07 mm	3.51 mm
Error in y	0.96 mm	2.13 mm	3.76 mm
Error in z	0.73 mm	1.60 mm	2.21 mm

4.5.4 Conclusion

In this section, we introduce a work realizing MOD and position prediction of coil at the same time, using input voltage and differential voltage of detection coils as the feature signals of the system. NN is used to solve MOD as classification problem and position prediction as regression problem. The results show that our methods have good performances of accuracy of MOD over 90% and prediction error of misalignment distance under 1 mm, at best. Some additional validations have been implemented. Without MOD, only focusing on the position prediction, the trained NN shows better performances compared to the simultaneous trained NN. On the other hand, by varying the size of metal object, the effect of noise in the training data is tested. It shows that though the influence of noise exists, there is not obvious performance degradation over trained NN, demonstrating the robustness of the proposed method in some extent.

Chapter 5 Conclusion

In this thesis, to develop the performance of WPT system, several works have been proposed, focusing on different problems, using different methods. In general, the development of WPT focus on the two following issues.

1. Maximize and maintain the transfer efficiency under different adverse conditions, such as coil-misalignment.
2. Ensure the safety of system. Minimize the effect of electromagnetic radiation to human body. Avoid the risk brought by invading foreign object.

Aiming to solve these problems, make WPT more dependable and robust, the following works have been introduced in this thesis.

5.1 Topology optimization for WPT coupler

In Chapter 2, several researches of optimization of magnetic core in WPT coupler have been introduced. Considering different shapes of coil, the shape of magnetic core around it is optimized using NGnet method to express the topology function, and revolutionary algorithm to solve the optimization problems. Especially, some of the works use coupling coefficient and leakage flux density as the objective functions together, in order to find designs realizing better transfer effect and safety at same time. The optimized results in each works are compared with reference model, which uses simple and typical design of magnetic core, and it shows that our optimized models obtain better performances on the objectives that they considered, in some extent.

5.2 Optimization for transmitting coils

In Chapter 3, the optimization for transmitting coils in WPT coupler is introduced. Focusing on the anti-misalignment of WPT system, a multi-layer coil system with misalignment-based

control-strategy are considered, and the shapes of the coils are optimized using target field method, where NGnet method is applied to express the coil shapes by topology function, so that the optimization problem can be solved in a similar way like the works in Chapter 2. Finally, the optimized model shows better anti-misalignment performance than a simple reference model, proving the effectiveness of the proposed method.

5.3 Metal object detection and position prediction

In Chapter 4, the attention is given to the safety issue of WPT system. Except for the leakage magnetic field that has been considered a lot in previous chapters, the risk of foreign metal object is required to be avoided by realizing MOD, to ensure the safety of WPT. Therefore, we proposed several works of MOD, using machine learning methods to treat MOD as a classification problem, considering different WPT system (with or without magnetic core). The results of simulations and experiments show the effectiveness of our method to distinguish the signal change brought by coil-misalignment and existence of metal object. Moreover, with the application of detection coils in WPT system, introducing more feature signals to represent the status of system, the position prediction is realized with MOD simultaneously, providing useful reference to adjust WPT system safer, and with better performance.

5.4 Future work

In Chapter 2 and Chapter 3, we have optimized the designs of magnetic core and coil in WPT coupler, respectively. But a simultaneous optimization of both has not yet been implemented. However, there is concern of complexity of optimization problem if consider these two objects together. Besides, as mentioned in Chapter 3, the misalignment-based control strategy still requires to be improved, which can be considered as a part in optimization as well.

On the other side, about the research of MOD and position prediction, the experimental validation of section 4.5 is still not finished. Especially, the noise effect on the method strongly

needs experiments to evaluate. Moreover, not only limited to the application in WPT, this idea of anomaly detection – extracting feature signals and processed by machine learning methods – can be adopted in other electric machine or system. We believe it will be, or has been, a major trendy of anomaly detection, and more works needs to be done for different specific scenarios.

References

[1] N. Tesla, “Transmission of electrical energy without wire”, *Elect. World Eng.*, vol. 1, pp.21-24, 1904.

[2] F. Lu, H. Zhang, & C. Mi, “A review on the recent development of capacitive wireless power transfer technology,” *Energies*, vol. 10, no. 11, pp. 1752, 2017.

[3] J. O. McSpadden, & J. C. Mankins, “Space solar power programs and microwave wireless power transmission technology,” *IEEE microwave magazine*, vol. 3, no. 4, pp. 46-57, 2002.

[4] D. van Wageningen and T. Staring, “The Qi wireless power standard,” *Proceedings of 14th International Power Electronics and Motion Control Conference EPE-PEMC 2010*, pp. S15-25-S15-32, 2010.

[5] T. Sato, K. Watanabe and H. Igarashi, “Multimaterial Topology Optimization of Electric Machines Based on Normalized Gaussian Network,” *IEEE Transactions on Magnetics*, vol. 51, no. 3, pp. 1-4, 2015.

[6] H.F. Leung, A.P. Hu, “Theoretical modeling and analysis of a wireless ultrasonic power transfer system,” *IEEE PELS workshop on emerging Technologies: wireless power (WoW)*, pp. 1-6, 2015.

[7] A. Massa, G. Oliveri, F. Viani, P. Rocca, “Array designs for long-distance wireless power transmission: state-of-the-art and innovative solutions,” *Proc. IEEE*, vol.101, no.6, pp. 1464-1481, 2013.

[8] W. Zhou, K. Jin, “Efficiency evaluation of laser diode in different driving modes for wireless power transmission,” *IEEE Trans. Power Electron.*, vol.30, no.11, pp. 6237-6244, 2015

[9] Y. Su, W. Zhou, A.P. Hu, C. Tang, S. Xie, Y. Sun, “Full-duplex communication on the shared channel of a capacitively coupled power transfer system,” *IEEE Trans. Power. Electron.*, vol.32, no.4, pp. 3229-3239, 2017.

[10] M. Budhia, G. A. Covic, J. T. Boys, “Design and optimization of circular magnetic structures for lumped inductive power transfer systems,” *IEEE Transactions on Power Electronics*, vol.26, no.11, pp. 3096-3108, 2011.

[11] M. Budhia, J. T. Boys, G. A. Covic, et al, “Development of a single-sided flux magnetic coupler for electric vehicle IPT charging systems,” *IEEE Transactions on Industrial*

Electronics, vol.60, no.1, pp. 318-328, 2011.

[12] R. Shimizu, Y. Kaneko and S. Abe, "A new he core transmitter of a contactless power transfer system that is compatible with circular core receivers and H-shaped core receivers," *2013 3rd International Electric Drives Production Conference (EDPC)*, pp. 1-7, 2013.

[13] E. G. Marques and A. M. S. Mendes, "Modelization and optimization of solenoid magnetic structures for IPT systems," *2017 11th IEEE International Conference on Compatibility, Power Electronics and Power Engineering (CPE-POWERENG)*, pp. 489-494, 2017.

[14] A. A. S. Mohamed, S. An and O. Mohammed, "Coil Design Optimization of Power Pad in IPT System for Electric Vehicle Applications," *IEEE Transactions on Magnetics*, vol. 54, no. 4, pp. 1-5, 2018.

[15] Z. Luo, X. Wei, M. G. S. Pearce and G. A. Covic, "Multiobjective Optimization of Inductive Power Transfer Double-D Pads for Electric Vehicles," *IEEE Transactions on Power Electronics*, vol. 36, no. 5, pp. 5135-5146, 2021.

[16] N. Tesla, "On light and other high frequency phenomena," *Journal of the Franklin Institute*, vol. 136, no.4, pp. 259-279, 1893.

[17] International Standard SAE J2954, "Wireless Power Transfer for Light-Duty Plug-In/Electric Vehicles and Alignment Methodology," 2020.

[18] IEC TS 61980-3, "Electric vehicle wireless power transfer (WPT) systems - Part 3: Specific requirements for the magnetic field wireless power transfer systems," 2019.

[19] W. Feng, X. C. Li, and W. Gu, "Compensation Parameters Optimization of Wireless Power Transfer for Electric Vehicles," *Electronics*, vol. 9, no. 5 :789, 2020.

[20] F. Lucchini, R. Torchio, V. Cirimele, P. Alotto and P. Bettini, "Topology Optimization for Electromagnetics: A Survey," *IEEE Access*, vol. 10, pp. 98593-98611, 2022.

[21] E. Hassan, E. Wadbro and M. Berggren, "Topology Optimization of Metallic Antennas," *IEEE Transactions on Antennas and Propagation*, vol. 62, no. 5, pp. 2488-2500, 2014.

[22] Y. Otomo and H. Igarashi, "A 3-D Topology Optimization of Magnetic Cores for Wireless Power Transfer Device," *IEEE Transactions on Magnetics*, vol. 55, no. 6, pp. 1-5, 2019.

[23] O. Sigmund, "A 99 line topology optimization code written in Matlab." *Struct. Multidisc. Optim.* vol. 21, no.2, pp. 120–127, 2001.

[24] M. Y. Wang, X. Wang, D. Guo, "A level set method for structural topology optimization," *Computer Methods in Applied Mechanics and Engineering*, Vol. 192, no. 1–2, pp. 227-246, 2003.

[25] K. Krishnakumar, "Micro-genetic algorithms for stationary and non-stationary function optimization," *Intelligent control and adaptive systems*, vol. 1196, pp. 289-296, 1990.

[26] K. Deb, A. Pratap, S. Agarwal, and T. Meyarivan, "A fast and elitist multiobjective genetic algorithm: NSGA-II," *IEEE transactions on evolutionary computation*, vol. 6, no. 2, pp.

182-197, 2002.

[27] L. J. Eshelman, and J. D. Schaffer, “RealCoded Genetic Algorithms and Interval-Schemata,” *Foundations of Genetic Algorithms*, vol. 2, pp. 187-202, 1993.

[28] F. Y. Lin, A. Zaheer, M. Budhia and G. A. Covic, “Reducing leakage flux in IPT systems by modifying pad ferrite structures,” *2014 IEEE Energy Conversion Congress and Exposition (ECCE)*, pp. 1770-1777, 2014.

[29] International Commission on Non-Ionizing Radiation Protection, “Guidelines for limiting exposure to time-varying electric and magnetic fields (1 Hz to 100 kHz),” *Health Phys.*, vol. 99, no. 6, pp. 818–836, 2010.

[30] T. Yilmaz, N. Hasan, R. Zane and Z. Pantic, “Multi-Objective Optimization of Circular Magnetic Couplers for Wireless Power Transfer Applications,” *IEEE Transactions on Magnetics*, vol. 53, no. 8, pp. 1-12, 2017.

[31] M. Budhia, G. A. Covic and J. T. Boys, “Design and Optimization of Circular Magnetic Structures for Lumped Inductive Power Transfer Systems,” *IEEE Transactions on Power Electronics*, vol. 26, no. 11, pp. 3096-3108, 2011.

[32] S. Jayalath and A. Khan, “Design, Challenges, and Trends of Inductive Power Transfer Couplers for Electric Vehicles: A Review,” *IEEE Journal of Emerging and Selected Topics in Power Electronics*, vol. 9, no. 5, pp. 6196-6218, 2021.

[33] S. Kim, G. A. Covic and J. T. Boys, “Tripolar Pad for Inductive Power Transfer Systems for EV Charging”, *IEEE Transactions on Power Electronics*, Vol. 32, No. 7, pp. 5045-5057, 2017.

[34] A. Foote, D. Costinett, R. Kusch, J. Pries, M. Mohammad and B. Ozpineci, “Fourier Analysis Method for Wireless Power Transfer Coil Design,” *2020 IEEE 21st Workshop on Control and Modeling for Power Electronics (COMPEL)*, pp. 1-8, 2020.

[35] L. K. Forbes and S. Crozier, “Novel target-field method for designing shielded biplanar shim and gradient coils,” *IEEE Transactions on Magnetics*, vol. 40, no. 4, pp. 1929-1938, 2004.

[36] T. Hirasawa, Y. Ishihara, “Gradient Coil Design Method for Handy MRI,” *World Congress on Medical Physics and Biomedical Engineering*, pp. 837-840, 2009.

[37] R. Turner, “A target field approach to optimal coil design”, *Journal of physics D: Applied physics*, Vol.19, No. 8, L147, 1986.

[38] T. Voß, N. Hansen, and C. Igel, “Improved step size adaptation for the MO-CMA-ES,” *Proceedings of the 12th annual conference on Genetic and evolutionary computation (GECCO '10)*, pp. 487–494, 2010.

[39] V. Väisänen, J. Hiltunen, J. Nerg and P. Silventoinen, “AC resistance calculation methods and practical design considerations when using litz wire,” *IECON 2013 - 39th Annual*

Conference of the IEEE Industrial Electronics Society, pp. 368-375, 2013.

[40] K. Jung, J. Park, S. Son and S. Ahn, "Position Prediction of Wireless Charging Electric Vehicle for Auto Parking using Extreme Gradient Boost Algorithm," *2020 IEEE Wireless Power Transfer Conference (WPTC)*, pp. 439-442, 2020.

[41] J. D. Hunter, "Matplotlib: A 2D graphics environment," *Computing in science & engineering*, Vol.9, No.3, pp. 90-95, 2007.

[42] F. A. Fortin, F. M. De Rainville, M. A. Gardner, "DEAP: Evolutionary Algorithms Made Easy," *Journal of Machine Learning Research*, Vol. 13, pp. 2171-2175, 2012.

[43] Y. Zhang, Z. Yan, J. Zhu, S. Li, C. Mi, "A review of foreign object detection (FOD) for inductive power transfer systems," *eTransportation*, vol. 1, 100002, 2019.

[44] L. Xiang, Z. Zhu, J. Tian and Y. Tian, "Foreign Object Detection in a Wireless Power Transfer System Using Symmetrical Coil Sets," *IEEE Access*, vol. 7, pp. 44622-44631, 2019.

[45] S. Y. Chu and A. -T. Avestruz, "Electromagnetic Model-Based Foreign Object Detection for Wireless Power Transfer," *2019 20th Workshop on Control and Modeling for Power Electronics (COMPEL)*, pp. 1-8, 2019.

[46] T. Poguntke, P. Schumann, & K. Ochs, "Radar-based living object protection for inductive charging of electric vehicles using two-dimensional signal processing," *Wireless Power Transfer*, vol. 4, no. 2, pp. 88-97, 2017.

[47] T. Sonnenberg, A. Stevens, A. Dayerizadeh and S. Lukic, "Combined Foreign Object Detection and Live Object Protection in Wireless Power Transfer Systems via Real-Time Thermal Camera Analysis," *2019 IEEE Applied Power Electronics Conference and Exposition (APEC)*, pp. 1547-1552, 2019.

[48] A. Berthault, D. Rousselle, G. Zerah, "Magnetic properties of Permalloy microparticles," *Journal of Magnetism and Magnetic Materials*, vol. 112, issue 1-3, pp. 477-480, 1992.

[49] S. B. Kotsiantis, I. D. Zaharakis, & P. E. Pintelas, "Machine learning: a review of classification and combining techniques," *Artificial Intelligence Review*, vol. 26, no. 3, pp. 159-190, 2006.

[50] M. Abadi, P. Barham, J. Chen, et al, "{TensorFlow}: a system for {Large-Scale} machine learning", *12th USENIX symposium on operating systems design and implementation (OSDI 16)*, pp. 265-283, 2016.

[51] F. Pedregosa, et al, "Scikit-learn: Machine learning in Python," *the Journal of machine Learning research*, vol. 12, pp. 2825-2830, 2011.

[52] C. Cortes, V. Vapnik, "Support-vector networks," *Machine learning*, vol. 20, no. 3, pp. 273–297, 1995.

[53] T. Hastie, R. Tibshirani, J. Friedman, "Boosting and additive trees". The elements of

statistical learning. Springer, New York, NY, pp. 337-387, 2009.

[54] Tin Kam Ho, "Random decision forests," *Proceedings of 3rd International Conference on Document Analysis and Recognition*, vol.1, pp. 278-282, 1995.

[55] D. P. Kingma, J. Ba, "Adam: A method for stochastic optimization," *arXiv preprint arXiv*, 1412.6980, 2014.

[56] S. Y. Jeong, H. G. Kwak, G. C. Jang, et al, "Dual-purpose nonoverlapping coil sets as metal object and vehicle position detections for wireless stationary EV chargers," *IEEE Transactions on Power Electronics*, vol. 33, no. 9, pp.7387-7397, 2017.

[57] J. Friedman, "Greedy function approximation: a gradient boosting machine," Annals of statistics, pp. 1189-1232, 2001.

[58] K. Jung, J. Park, S. Son and S. Ahn, "Position prediction of wireless charging electric vehicle for auto parking using extreme gradient boost algorithm," *2020 IEEE Wireless Power Transfer Conference (WPTC)*, 2020.

[59] S. Son et al., "Foreign object detection of wireless power transfer system using sensor coil," *2021 IEEE Wireless Power Transfer Conference (WPTC)*, 2021.

Acknowledgement

Sincere thanks to all those who helped me during the writing of this thesis.

First and foremost, I would like to thank my research supervisor, Prof. Hajime Igarashi, Course of Systems Science and Informatics, Graduate School of Information Science and Technology, Hokkaido University, for his kind guidance and advice on both research and life. I also want to thank associate Professor So Noguchi for his help and kindness.

Secondly, thanks to all the members in laboratory, for their help and making the laboratory's atmosphere so lively. Specially thanks to my tutor Yoshitsugu Otomo, for his patient guidance on researches. Besides, gratitude to Mrs. Naoshiyo Saito and Mr. Atsushi Imai, for their supports to this laboratory. Nothing can replace your works for everyone's researches.

And I appreciate my friends Hou and Wen, for continuing research career as PhD student, same with me, lol.

A special gratitude part to those artists who appeared in my life and gave me support or comfort in any form. Thanks to Mayday, Eve Ai, Wyman wong, albert leung and Jun Togawa. Your works gave me comfort during these years in Japan. Gratitude to Yukio Mishima, Flannery O'Connor and Masaaki Yuasa for that your works changed my life greatly. A mourning to Kyoto Animation, you will never be forgotten. Specially appreciate the supports over the years, from works by Yuu Asakura, Akiho Yoshizawa, Arina Hashimoto and Minami Aizawa.

Last, thanks my parents H. Gong and Z. Zhou, for their support and understanding to my abroad study. Thanks to my cats, and elainisel, nothing could compare to that you have ever been in my life.

Above is almost what I wrote in the acknowledgement in my master thesis, three years ago. For the human world, the past three years may be a period of great change, which probably continues, or even worsen. Countless people's life and living were facing with great shock in many respects. We were forced to change ourselves to adapt, or just accept sorrow.

I decided to kept most of the acknowledgement unchanged, for the invariable gratitude and mood in my life. No matter how the world changes, the precious part within ourselves, will not change, and fade. Just keep them, and keep witnessing the era. Even if we don't arrive a better world in the end, at least there is something to be yarned.

However, I want to add someone in this acknowledgement who intruded into my life in recent years, lol. Thanks to Yoyo Sham, Jay Fung, and Jianqing Li, for arousing and saving my nostalgia. Thanks to Hideaki Anno, words cannot express how your works changed my life. I have experienced, I have left. Thanks to what once appeared there.

Research Achievements

Journal

[1] Z. Zhang, Y. Guo, F. Li, **Y. Gong**, X. Liao, "A sandwich-type thermoelectric microwave power sensor for GaAs MMIC-compatible applications," *IEEE Electron Device Letters*, vol.37, no.12, pp. 1639-1641, 2016.

[2] **Y. Gong**, Y. Otomo, H. Igarashi, "Multi-objective topology optimization of magnetic couplers for wireless power transfer," *International Journal of Applied Electromagnetics and Mechanics*, vol. 64, no. 1-4, pp. 325-333, 2020.

[3] **Y. Gong**, Y. Otomo, H. Igarashi, "Sensorless metal object detection for wireless power transfer using machine learning," *COMPEL-The international journal for computation and mathematics in electrical and electronic engineering*, Vol .41, No. 3, pp. 807-823, 2021.

[4] **Y. Gong**, Y. Otomo, H. Igarashi, "Machine Learning Based Metal Object Detection for Wireless Power Transfer Using Differential Coils," *Journal of Advanced Simulation in Science and Engineering*, vol.9, no.1, pp. 20-29, 2022.

[5] **Y. Gong**, Y. Otomo, H. Igarashi, "Neural Network for Both Metal Object Detection and Coil Misalignment Prediction in Wireless Power Transfer," *IEEE Transactions on Magnetics*, vol.58, issue 9, 2022.

[6] Q. Liu, Y. Otomo, **Y. Gong**, H. Igarashi, "Equivalent Circuit of High Frequency Inductor to Consider Eddy Currents and Resonance," *International Journal of Applied Electromagnetics and Mechanics*, [accepted].

International conference

[1] Y. Otomo, **Y. Gong**, H. Igarashi, "3-D Topology Optimization of Magnetic Cores for Wireless Power Transfer with Double-Sided Winding Coils," *OIPE2018*, Oral Session 5-3, Hall in Tirol, Austria, September, 2018.

[2] **Y. Gong**, Y. Otomo, H. Igarashi, "Multi-Objective Topology Optimization of Circular Magnetic Couplers for Wireless Power Transfer," *ISEM2019*, 80, Nanjing, China, Sep., 2019.

[3] **Y. Gong**, Y. Otomo, H. Igarashi, "Sensorless Metal Object Detection for Wireless Power Transfer Using Machine Learning," *19th International IGTE Symposium on Numerical Field Calculation in Electrical Engineering (IGTE2020)*, on-site and online, 20-23 Sep., 2020.

[4] **Y. Gong**, Y. Otomo, H. Igarashi, "Analysis of Foreign Object Detection for Wireless power

transfer Using Differential Coils," *The 40th JSST Annual International Conference on Simulation Technology (JSST2021)*, pp.257-260, Sep., 2021.

[5] **Y. Gong**, Y. Otomo, H. Igarashi, "Metal Object Detection for Wireless Power Transfer Using Differential Coils Based on Neural Network," *Proc.COMPUMAG2021*, PC-A2-7, Jan., 2022.

[6] Q. Liu, Y. Otomo, **Y. Gong**, H. Igarashi, "Equivalent Circuit of High Frequency Inductor to Consider Eddy Currents and Resonance," *ISEM2022, 216*, Thessaloniki, Greece, Jun., 2022.

Domestic conference

[1] **Y. Gong**, Y. Otomo, H. Igarashi, "3-D Topology Optimization of Magnetic Cores for Wireless Power Transfer Device Using Genetic Algorithm," *平成30年電気学会C部門大会*，SS2-4，札幌，9月，2018.

[2] **Y. Gong**, Y. Otomo, H. Igarashi, "3-D Topology Optimization of Magnetic Cores for Wireless Power Transfer with Double-D Coils Using Genetic Algorithm," *平成30年度電気・情報関係学会北海道支部連合大会*，1，札幌，10月，2018.

[3] **Y. Gong**，Y. Otomo，H. Igarashi, "Multi-Objective Topology Optimization of Magnetic Couplers for Wireless Power Transfer Device," *2019年電気学会産業応用部門大会*，Y-26，長崎，8月，2019.

[4] **Y. Gong**，Y. Otomo，H. Igarashi, "Basic study on sensorless metal object detection in wireless power transfer system using neural network," *電気学会静止器回転機合同研究会*, SA-20-040, RM-20-064, 2020.

[5] **Y. Gong**，H. Igarashi, "Optimization of multi-layer coils for wireless power transfer considering misalignment," *第35回計算力学講演会（CMD2022）*, 11月， 2022.